Modelling the spatial and temporal constrains of the GABAergic influence on neuronal excitability

Short title: Spatial constrains of GABAergic rheobase shift

Aniello Lombardi, Heiko J. Luhmann, Werner Kilb

Institute of Physiology, University Medical Center of the Johannes Gutenberg University, Duesbergweg 6, 55128 Mainz, Germany

Corresponding author: wkilb@uni-mainz.de;
Tel.: +49-211-3926101,
ORCID: 0000-0001-8204-3984

Abstract:

GABA (γ-amino butyric acid) is an inhibitory neurotransmitter in the adult brain that can mediate depolarizing responses during development or after neuropathological insults. Under which conditions GABAergic membrane depolarizations are sufficient to impose excitatory effects is hard to predict, as shunting inhibition and GABAergic effects on spatiotemporal filtering of excitatory inputs must be considered. To evaluate at which reversal potential a net excitatory effect was imposed by GABA (E_{GABA}^{Thr}), we performed a detailed in-silico study using simple neuronal topologies and distinct spatiotemporal relations between GABAergic and glutamatergic inputs.

These simulations revealed for GABAergic synapses located at the soma an E_{GABA}^{Thr} close to action potential threshold (E_{AP}^{Thr}), while with increasing dendritic distance E_{GABA}^{Thr} shifted to positive values. The impact of GABA on AMPA-mediated inputs revealed a complex temporal and spatial dependency. E_{GABA}^{Thr} depends on the temporal relation between GABA and AMPA inputs, with a striking negative shift in E_{GABA}^{Thr} for AMPA inputs appearing after the GABA input. The spatial dependency between GABA and AMPA inputs revealed a complex profile, with E_{GABA}^{Thr} being shifted to values negative to E_{AP}^{Thr} for AMPA synapses located proximally to the GABA input, while for distally located AMPA synapses the dendritic distance had only a minor effect on E_{GABA}^{Thr}. For tonic GABAergic conductances E_{GABA}^{Thr} was negative to E_{AP}^{Thr} over a wide range of g_{GABA}^{tonic} values. In summary, these results demonstrate that for several physiologically relevant situations E_{GABA}^{Thr} is negative to E_{AP}^{Thr}, suggesting that depolarizing GABAergic responses can mediate excitatory effects even if E_{GABA} did not reach E_{AP}^{Thr}.

Author summary:

The neurotransmitter GABA mediates an inhibitory action in the mature brain, while it was found that GABA provokes depolarizations in the immature brain of after neurological insults. It is, however, not clear to which extend these GABAergic depolarizations con contribute to an excitatory effect. In the present manuscript we approached this question with a computational model of a simplified neurons to determine which amount of a GABAergic depolarizing effect, which we quantified by the so called GABA reversal potential (E_{GABA}), was required to turn GABAergic inhibition to excitation. The results of our simulations revealed that if GABA was applied alone a GABAergic excitation was induced when E_{GABA} was around the action potential threshold. When GABA was applied together with additional excitatory inputs, which is the physiological situation in the brain, only for spatially and temporally correlated inputs E_{GABA} was close to the action potential threshold. For situations in which the additional excitatory inputs appear after the GABA input or are distant to the GABA input, an excitatory effect of GABA could be observed already at E_{GABA} substantially negative to the action potential threshold. This results indicate that even slightly depolarizing GABA responses, which may be induced during or after neurological insults, can potentially turn GABAergic inhibition into GABAergic excitation.

1. Introduction

The neurotransmitter γ-amino butyric acid (GABA) is the major inhibitory neurotransmitter in the adult mammalian brain [1]. GABA regulates the excitation of neurons and is thus essential for e.g. the control of sensory integration, regulation of motor functions, generation of oscillatory activity, and neuronal plasticity [2–4]. GABA mediates its effects via metabotropic $GABA_B$ receptors [5] and ionotropic $GABA_A$ receptors, ligand-gated anion-channels with a high Cl^- permeability and a partial HCO_3^- permeability [6]. The membrane responses caused by $GABA_A$ receptor activation thus depend on the reversal potential of GABA receptors (E_{GABA}), which is determined mainly by the intracellular Cl^- concentration ($[Cl^-]_i$) and to a lesser extent by the HCO_3^- gradient across the membrane [6].

About 30 years ago seminal studies demonstrated that $GABA_A$ receptors can mediate depolarizing and excitatory actions in the immature central nervous system [7–9]. This depolarizing GABAergic action reflects differences in the $[Cl^-]_i$ homeostasis between immature and adult neurons [10–15]. In particular, low functional expression of a K^+-Cl^- cotransporter (KCC2), which mediates the effective extrusion of Cl^- and thus establishes the low $[Cl^-]_i$ required for hyperpolarizing GABAergic membrane responses [16], prevent hyperpolarizing GABA responses in the immature brain. In addition, the inwardly directed Cl^- transporter NKCC1 mediates the accumulation of Cl^- above passive distribution that underlies the depolarizing membrane responses upon activation of $GABA_A$ receptors [17–21]. These depolarizing GABAergic membrane responses play a role in several developmental processes [11,22,23], like neuronal proliferation [24], apoptosis [25], neuronal migration [26], dendro- and synaptogenesis [27], timing of critical periods [28] and the establishment of neuronal circuitry [29]. Of clinical importance, an elevated $[Cl^-]_i$ is also a typical consequence of several neurological disorders in

the adult brain, like trauma, stroke or epilepsy and is considered to augment the consequences of such insults [11,30,31].

However, it is important to consider that depolarizing GABA responses do not per se lead to excitatory effects. In fact, the membrane shunting that unescapably accompanies the activation of $GABA_A$ receptors can dominate over the excitatory effects of the membrane depolarization [11,32–34]. Theoretical considerations [35,36] suggest that the relation between E_{GABA} and the action potential threshold (E_{AP}^{Thr}) determine whether activation of $GABA_A$ receptors mediates excitatory (E_{GABA} positive to E_{Thr}^{AP}) or inhibitory (E_{GABA} negative to E_{Thr}^{AP}) actions. However, this concept is probably an oversimplification, as within the dendritic compartment the local activation of GABAergic conductance influences not only the amplitude of local excitatory synaptic postsynaptic potentials (EPSPs), but also the length and time constants of the dendritic membrane and thus temporal and spatial summation of excitatory synaptic inputs [37,38]. Moreover, the depolarizing effect of GABAergic stimulation outlasts the conductance increase associated with $GABA_A$ receptor activation, resulting in a bimodal GABA effect. Close to the initiation of GABAergic responses the shunting effect of the enhanced GABAergic conductance dominate and mediate inhibition. This phase is followed by an excitatory phase dominated by the GABAergic depolarization [39,40]. In addition, E_{Thr}^{AP} is a dynamic variable, that depends on the background conductance and the density and adaptation state of voltage-gated Na^+ channels [10,41,42]. Experimental studies on the effects of GABAergic inputs on neuronal excitability demonstrated for immature neocortical neurons that E_{GABA} required for excitatory GABAergic responses (E_{GABA}^{Thr}) was close to E_{AP}^{Thr} [43], while in immature hippocampal neurons E_{GABA}^{Thr} was considerably negative to E_{AP}^{Thr} [44]. The observations that (i) the GABA effect can switch from inhibition to excitation for delayed glutamatergic inputs [39], that (ii) GABA inputs in distal dendrites can facilitate neuronal excitability [40], and that (iii) extrasynaptic GABAergic

activation mediates an excitatory effect whereas synaptic inputs mediate inhibition [45], also suggest that the reversal potential required for GABAergic excitation is not only defined by E_{AP}^{Thr}. This complexity is further supported by recent in-vivo investigations that identified excitatory as well as inhibitory effects of GABA in the immature brain [46–48]. In summary, to our knowledge no clear concept is currently available that can explain how E_{GABA} influences GABAergic excitation/inhibition and the effect of GABA on spatiotemporal summation of EPSPs in the dendritic compartment.

Therefore, the present computational study investigates the dependency between E_{GABA} and excitatory and inhibitory consequences of $GABA_A$ receptor activation and attempts to establish a general view of the impact of depolarizing GABAergic effects on the excitability of neurons. Our results demonstrate that only for GABAergic synapses located at or close to the soma the difference between E_{GABA} and E_{AP}^{Thr} predicts whether GABA has an excitatory or an inhibitory action. The E_{GABA} at which depolarizing GABA actions switch from inhibition to excitation is in most cases negative to E_{AP}^{Thr} and depends on the temporal and spatial relation between GABA and AMPA inputs, with a more excitatory effect on AMPA inputs that are delayed or located proximal to GABA inputs. We conclude from our results that GABA can mediate excitatory effects even if E_{GABA} is considerably hyperpolarized to E_{AP}^{Thr}.

2. Results

2.1. Simulation of active and passive properties of immature CA3 pyramidal neurons

The parameters used for the models in this study are based on the cellular properties obtained in whole-cell patch-clamp recordings from visually identified CA3 neurons in horizontal hippocampal slices from P4-7 mice. Some parameters of these recordings have been used in our previous report [49]. The analysis of the patch-clamp experiments revealed that the immature CA3 pyramidal neurons had an average resting membrane potential (RMP) of −50.5 ± 1.3 mV, an average input resistance (R_{Inp}) of 1.03 ± 0.11 GOhm, and an average membrane capacity (C_M) of 132.3 ± 33.6 nF (all n=42). As the passive membrane properties directly influence synaptic integration as well as active properties, like E_{AP}^{Thr} or the shape of the action potential (AP), we first adapted the spatial properties and the passive conductance g_{pas} of the ball-and-stick model to emulate the recorded properties. To obtain sufficient similarity for these parameters between the model and the real cells we equipped a ball-and-stick model (soma diameter (d) = 46.6 µm, dendrite length = 1 mm, dendrite diameter = 1 µm) with a passive conductance density (g_{pas}) of $1.28*10^{-5}$ nS/cm^2 at a reversal potential (E_{pas}) of −50.5 mV. This model had a RMP of -50.5 mV, a R_{Inp} of 1.045 GOhm and a C_M of 144.4 nF. In some experiments we reduced the topology to a simple ball model (*one node, d* = 46.6 µm), without adapting g_{pas}, to evaluate the impact of GABA under quasi one-dimensional conditions.

With these configurations we next implemented a mechanism that provided APs with properties comparable to the APs recorded in CA3 pyramidal neuron. In particular, we were interested to simulate the AP properties around AP initiation as precisely as possible, because for the main questions of this manuscript we are interested in the E_{AP}^{Thr}. Since it was not possible to generate a reasonable sharp AP onset with a standard Hodgkin-Huxley (HH) model, we used a modified

Markov model (see materials for details) to simulate AP with a considerable precision (Fig. 1A-E).

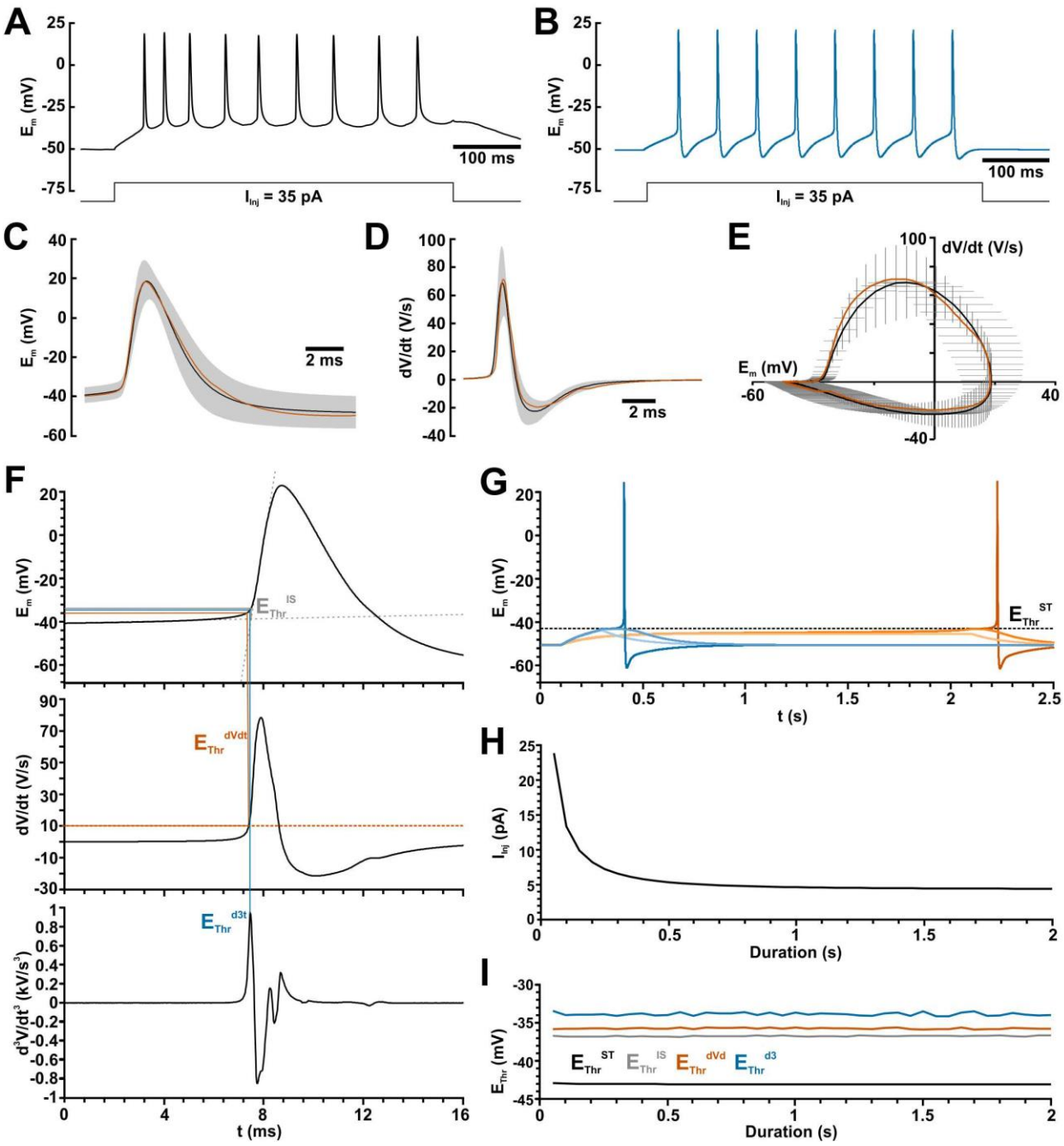

Figure 1. *Properties of recorded and simulated action potentials (APs). A: Typical AP train recorded in a CA3 pyramidal neuron upon a current injection of +35 pA. B: AP train simulated in a ball-and-stick model using the modified Markov model. C: Average voltage trace of*

recorded APs (black line = average; gray area ± SEM) and of the simulated AP (orange trace). D: Discharge rate of recorded (black line, gray area) and simulated AP (orange trace). E: Phase plane plot of recorded (whiskers = mean ± SEM) and simulated AP (orange trace). F: Determination of the AP threshold from the intersection of linear voltage fits (E_{Thr}^{IS}, gray lines), from the time point dV/dt reaches the 10 V/s threshold (E_{Thr}^{dVdt}, orange lines), and from the time point d^3V/dt^3 reaches the peak value (E_{Thr}^{d3}, blue lines). G: Determination of the AP threshold at maximal potential of a subthreshold depolarization (E_{Thr}^{ST}, black lines). Blue traces indicate a 200 ms depolarizing stimulus and orange traces a 2 s stimulus. Dark tones indicate the smallest suprathreshold stimulus, middle tones the largest subthreshold stimulus and light tones a clearly subthreshold stimulus. H: Injection current (I_{Inj}) required to elicit an AP at different stimulus durations. I: Values of different AP threshold parameters for various stimulation durations. Note that AP threshold is independent from the stimulation duration.

Because the relation between E_{AP}^{Thr} and E_{GABA} is one major parameter investigated in this study and since no clear definition of the AP threshold has been given [42], we initially used 4 different methods to determine the action potential threshold (Fig. 1F): 1.) The AP threshold value E_{Thr}^{dVdt} was defined as the potential at which dV/dt first crosses a velocity of 10 V/s [44,50] (Fig. 1F orange lines). 2.) E_{Thr}^{d3} was defined as the potential at the time point of the first positive peak in d^3V/dt^3 [51] (Fig. 1F, blue lines). 3.) E_{Thr}^{IS} was determined at the intersection between linear regressions of the baseline before the AP and the rising phase of an AP (Fig. 1H) [43] (Fig. 1F, gray lines). 4.) E_{Thr}^{ST} was defined as the maximal potential reached at the strongest subthreshold stimulation (Fig. 1G, dashed line), i.e. the minimal potential that did not lead into the regenerative Hodgkin cycle. While the rheobase, i.e. the minimal suprathreshold injection current, demonstrated as expected a hyperbolic increase at shorter stimulus durations and converged to 4.4495 pA (Fig. 1H), the distinct E_{AP}^{Thr} parameters are virtually independent on the duration of

the stimulus (Fig. 1I). In the ball model average E_{Thr}^{dVdt} was −35.7 mV, average E_{Thr}^{d3} was −33.8 mV, average E_{Thr}^{IS} was −36.7 mV, and E_{Thr}^{ST} converged to −43.04 mV (Fig. 1I). When using the ball-and-stick model the rheobase was slightly larger at 6.708 pA, E_{Thr}^{dVdt} was −35.7 mV, E_{Thr}^{d3} was −33.8 mV, E_{Thr}^{IS} was −36.6 mV, and E_{Thr}^{ST} converged to −42.71 mV (data not shown).

Because for the following simulations several hundred sweeps were required for each analyzed parameter and thus a time-effective simulation was compulsory, we next evaluated the maximal dt interval required to obtain stable AP responses. This experiment demonstrated that the time course of AP and E_{AP}^{Thr} determination remained stable until a dt of 0.1 ms (Suppl. Fig. 1). Thus we decided to use a dt of 0.1 ms in the following simulations.

2.2. Determination of the threshold for excitatory GABAergic responses

To identify the reversal potential at which the GABA response switches from inhibitory to excitatory, we first determined the GABAergic conductance that was sufficient to trigger an AP, which was defined as the GABAergic excitation threshold (g_{GABA}^{Thr}). The value of g_{GABA}^{Thr} was determined by systematically increasing the conductance of a simulated GABAergic input until an AP was evoked. To determine this excitation threshold as precisely as possible, we used a multi-step procedure to incrementally confine the threshold conductance (Fig. 2A). This procedure was repeated for a whole set of E_{GABA} values (Fig. 2B).

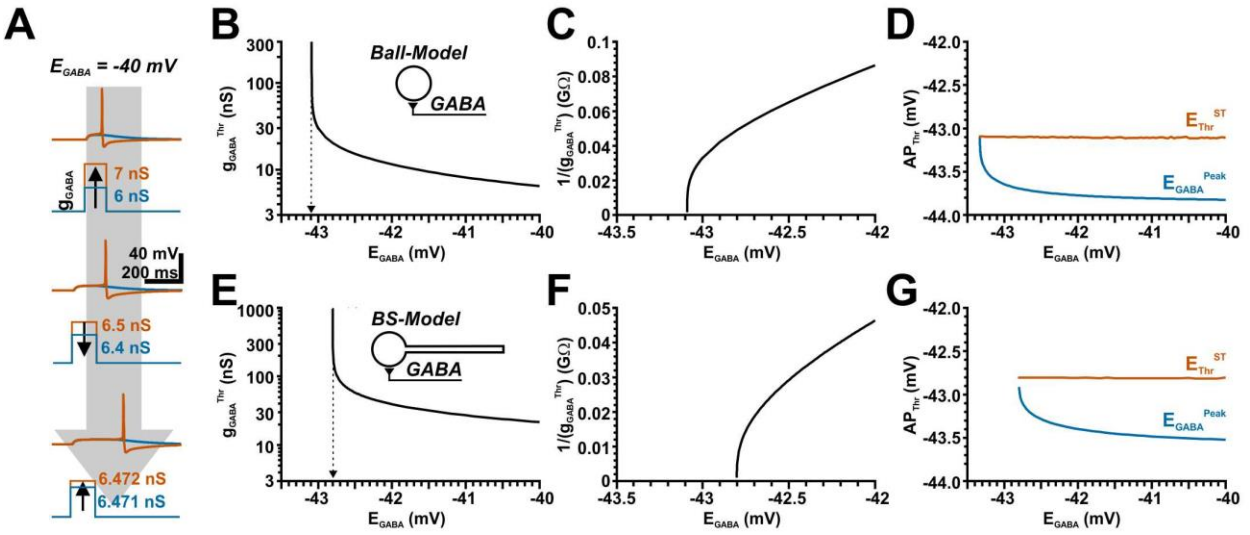

Figure 2. *Determination of the threshold conductance at different* E_{GABA} *enable the identification of* E_{GABA} *at which responses switch from inhibitory to excitatory (*E_{GABA}^{Thr}*). A: Typical voltage traces illustrating the mechanisms used to determine the threshold* g_{GABA} *value. For this purpose,* g_{GABA} *was increased until the first AP was induced (upper panel), then decreased by finer* g_{GABA} *steps until the AP disappears (middle panel), followed by a subsequent increase in* g_{GABA} *with finer* g_{GABA} *steps (lower panel). In total, 6 alternating rounds of increased/decreased* g_{GABA} *steps were used. The* g_{GABA} *value required to induce an AP in the last increasing step was considered as threshold (*g_{GABA}^{Thr}*). B: Plotting* g_{GABA}^{Thr} *versus* E_{GABA} *demonstrate that with decreasing* E_{GABA} *higher* g_{GABA}^{Thr} *values were required, which approximated infinite values. C: A reciprocal plot of* g_{GABA}^{Thr} *enables the precise determination of* E_{GABA}^{Thr}*. At* E_{GABA} *values negative to* E_{GABA}^{Thr} *no action potential could be induced, suggesting a stable GABAergic inhibition. D: The determined AP threshold* E_{Thr}^{ST} *(orange line) is constant over various* E_{GABA}*, whereas the peak potential of the GABAergic depolarization, which was determined at* g_{GABA}^{Thr} *in absence of AP mechanism (*E_{GABA}^{Peak}*, blue line) increases with decreasing* E_{GABA}*. Note that the values converged in one point when* E_{GABA} *reaches* E_{Thr}^{ST}*.*

E-G: Similar plots for a ball-and-stick model. Note that E_{GABA}^{Thr} was shifted to less negative values in this configuration.

In the ball model (*one node, d* = 46.6 µm) these systematic simulations demonstrated an obvious hyperbolic increase of g_{GABA}^{Thr} when E_{GABA} approaches values below −43 mV (Fig. 2B). The g_{GABA}^{Thr} curve approximated an E_{GABA} of −43.09 mV, which was precisely determined from a reciprocal plot of the g_{GABA}^{Thr} values (Fig. 2C). Negative to an E_{GABA} of −43.09 mV no action potential could be evoked, regardless of the amount of g_{GABA}. These E_{GABA} values thus reflects the threshold, at which GABA actions can mediate a direct excitation and we termed this value "threshold E_{GABA}" (E_{GABA}^{Thr}). Note that this value is close to the E_{Thr}^{ST} value of −43.04 mV determined in the previous experiments. Since E_{AP}^{Thr} is influenced directly by the total membrane conductance, we also determined the amplitude of the GABAergic voltage response under conditions when the AP initiation was blocked (E_{GABA}^{Peak}) as well as different E_{AP}^{Thr} parameters. These analyses revealed that E_{Thr}^{d3} was around −29 mV for all E_{GABA}. E_{Thr}^{ST} was relatively stable around −43.1 mV, with a slight positive shift at low E_{GABA} values that converges to −43.09 mV (Fig. 2D). E_{GABA}^{Peak} was for higher E_{GABA} around −43.8 mV and showed a positive shift with decreasing E_{GABA} that converged to values of −43.1 mV (Fig. 2D).

In summary, these results indicate that GABA acts as excitatory neurotransmitter as long as E_{GABA} is positive to −43.09 mV, which is extremely close to the AP threshold E_{Thr}^{ST}. This observation is in line with previous predictions that propose exactly this relation between E_{AP}^{Thr} and E_{GABA} [35,36]. In addition, our simulations suggest that E_{Thr}^{ST} is probably the most relevant definition for E_{AP}^{Thr} if the direction of GABA effects should be predicted from the difference between E_{GABA} and E_{AP}^{Thr}.

Next we performed the same simulation with a ball-and-stick model. These simulations revealed that the g_{GABA}^{Thr} curve approximated an E_{GABA} of −42.8 mV (Fig. 2E-F), which is in the range of the E_{Thr}^{ST} (−42.71 mV) determined for the ball-and-stick model. E_{Thr}^{d3} was around −29.8 mV for all E_{GABA}. E_{Thr}^{ST} was stable at values around −42.8 mV and converges at low E_{GABA} to −42.8 mV (Fig. 2G). E_{GABA}^{Peak} was for higher E_{GABA} around −43.6 mV and converged with decreasing E_{GABA} to −42.8 mV (Fig. 2G). Thus, E_{GABA}^{Thr} for a somatic synapse is still in good agreement with the AP threshold value E_{Thr}^{ST} with this slightly more complex neuronal topology.

For the next set of experiments, we located a single GABA synapse along the dendrite of the ball-and-stick model and determined E_{GABA}^{Thr} for each of these 20 synaptic positions, using the method described above. The considerable conductance and capacitance provided by the dendritic membrane leads, as expected, to a reduced amplitude and a slower time course of the GABAergic PSPs recorded at the dendritic positions (Fig. 3A). Accordingly, larger g_{GABA} values were required to trigger APs for more distant dendritic locations of GABAergic inputs (Fig. 3B, C). At the most distant dendritic positions g_{GABA} values above 100 nS (i.e. more than 100x of g_{GABA} of a single synaptic event [49]) were required to trigger an AP, which virtually clamped the dendritic membrane at the synapse position to E_{GABA} (Fig. 3B). A systematic analysis of g_{GABA}^{Thr} at different E_{GABA} values illustrated that g_{GABA}^{Thr} showed a considerable less steep dependency on E_{GABA} at more distant dendrite positions (Fig. 3C). The reciprocal plot of g_{GABA}^{Thr} demonstrated that the g_{GABA}^{Thr} values did not converge at similar E_{GABA} values for the different synapse locations, but that the curves reached the abscissa at considerable more positive values for distant GABAergic inputs (Fig. 3D). Intriguingly, E_{GABA}^{Thr} values were close to E_{Thr}^{ST} for synapses close to the soma, were shifted to slightly more negative E_{GABA}^{Thr} values for dendritic synapses at a distance of ca. 250 µm, and increased to more positive E_{GABA}^{Thr} values with additional distance to the soma (Fig. 3E). E_{GABA}^{Peak}, which was determined in the absence of AP mechanisms and reflects the effective

voltage fluctuation at the soma and thus the AP initiation site, was shifted to negative potentials at more distant dendritic positions (Fig. 3G, H), while the position of GABA synapses had no major effect on E_{Thr}^{ST} (Fig. 3F, H). In summary, these simulations revealed that E_{GABA}^{Th} is not close to the AP threshold value E_{Thr}^{ST} for synapses that are located in the dendrite, but that E_{GABA}^{Th} is shifted to more positive values with increasing distance. This observation suggests that for dendritic synapses a more positive E_{GABA} (corresponding to a higher $[Cl^-]_i$) is required to mediate a direct excitatory effect.

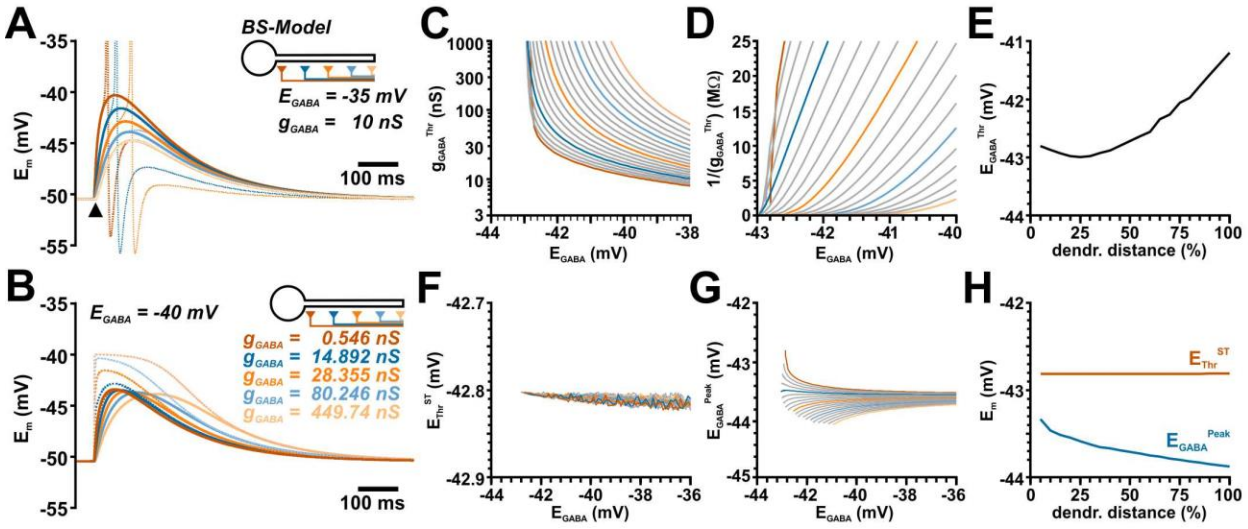

Figure 3. *Determination of E_{GABA}^{Thr} at different dendrite positions. A: Simulated voltage traces obtained with the given parameters at different locations as indicated by color code. The dashed traces represent simulation with added AP mechanism. The amplitude of GABA responses clearly depends on the dendritic location. B: Simulated voltage traces for g_{GABA}^{Thr} and E_{GABA} of -40 mV at the soma (solid trace) and the synaptic site (dashed line). Color codes the different synapse locations. For each location different g_{GABA} (as indicated) had to be used. Note that at distant synapses considerable large g_{GABA} were required, which virtually clamped E_m at the synaptic site to E_{GABA}. C: Systematic plot of g_{GABA}^{Thr} determined at various E_{GABA}. The curves were obtained from 20 equidistant positions along the dendrite. The 1th, 5th, 10th, 15th and 20th trace is color-coded as in A for better readability. D: The reciprocal plot of g_{GABA}^{Thr} revealed that the curves did not monotonically approach the abscissa. Therefore, E_{GABA}^{Thr} was estimated from a linear fit to the last two data-points. E: E_{GABA}^{Thr} showed a considerable shift towards*

depolarized potentials with increasing dendritic distance. F: The AP threshold E_{Thr}^{ST} remained rather stable with different E_{GABA} or different synaptic location. G: The peak potential (E_{GABA}^{Peak}) of the somatic GABAergic depolarization at g_{GABA}^{Thr} converges toward E_{Thr}^{ST} only for soma-near synapses (dark orange trace). With more distant synapses less depolarized E_{GABA}^{Peak} was required. Color code as in C. H: While the average E_{Thr}^{ST} (orange line) is stable for all dendritic locations, the average E_{GABA}^{Peak} (blue line) is shifted to more negative values with increasing dendritic distance.

2.3. Effect of phasic GABAergic inputs on glutamatergic excitation

The previous results demonstrated that only at perisomatic synapses E_{GABA}^{Thr} was reached when E_{GABA} was at the action potential threshold E_{Thr}^{ST}, but that E_{GABA}^{Thr} was systematically shifted to positive E_{GABA} at distant synapses in a ball-and-stick model. However, these experiments do not reflect the physiological situation of GABAergic transmission in the brain. First, the threshold conductance g_{GABA}^{Thr} determined by these simulations is above physiological values for moderate GABAergic inputs [49,52,53] making a direct excitatory GABAergic input implausible. And second, synaptic activity is characterized by the co-activation of GABA and glutamate receptors [54–56], with the latter constituting the main excitatory drive [57]. Therefore, we next simulated the impact of a GABAergic co-stimulation on glutamatergic synaptic inputs and determined the g_{AMPA} values that were required to trigger an AP. As in the previous experiments, we varied E_{GABA} to determine E_{GABA}^{Thr}, which is defined as the E_{GABA} value at which the GABAergic effect shifts from inhibitory (i.e. GABA co-activation requires larger g_{AMPA} to trigger APs) to excitatory action (i.e. GABA co-activation requires less g_{AMPA}) (Fig. 4A). This effect was quantified as the GABAergic excitability shift (Δg_{AMPA}^{Thr}), with g_{AMPA}^{Thr} describing the g_{AMPA} value sufficient to trigger an AP, and Δg_{AMPA}^{Thr} defined as difference in g_{AMPA}^{Thr} between conditions with and without GABAergic co-stimulation [$\Delta g_{AMPA}^{Thr} = (g_{AMPA}^{Th})_{withGABA} - (g_{AMPA}^{Th})_{w/oGABA}$].

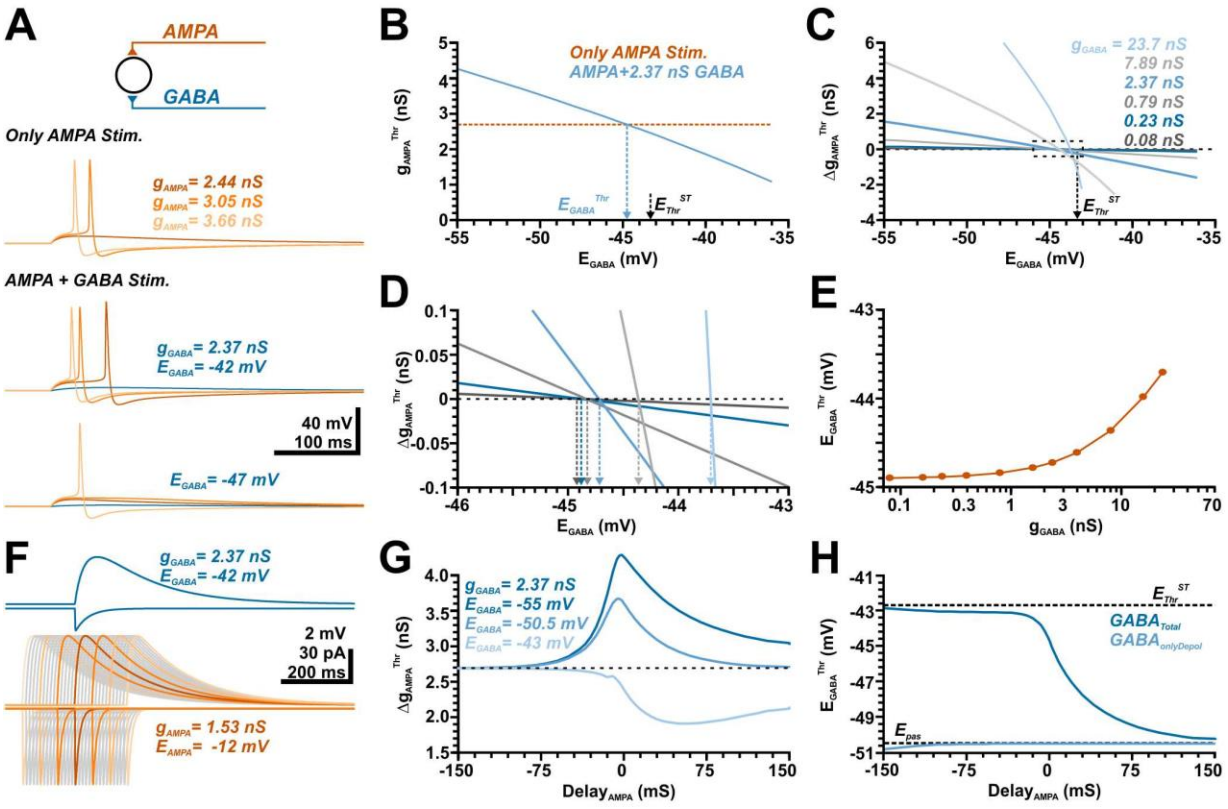

Figure 4. *Influence of a GABAergic input at different E_{GABA}^{Thr} on the AMPA receptor-dependent excitation threshold. A: Simulated voltage traces illustrating the membrane responses induced by three different conductances of the AMPA synapse in the absence (top traces) and the presence of a simultaneous GABAergic input at E_{GABA} of -42 mV (middle traces) and -47 mV (lower traces). B: Plot of the minimal g_{AMPA} required to trigger an AP (g_{AMPA}^{Thr}) versus the E_{GABA} of the synchronous GABA input (g_{GABA} = 2.37 nS). The E_{GABA} value at which this curve intersects with g_{AMPA}^{Thr} determined in the absence of GABA (orange line) defines the GABA concentration at which GABA switches from excitatory to inhibitory (E_{GABA}^{Thr}). C: Plot of Δg_{AMPA}^{Thr} versus E_{GABA} for different g_{GABA} values, as indicated in the graph. D: A magnification of the marked area in C allows the determination of E_{GABA}^{Thr} for the different g_{GABA}, color code as indicated in C. E: Plot of the E_{GABA}^{Thr} determined at different g_{GABA}. Note that E_{GABA}^{Thr} is substantially negative to E_{Thr}^{ST} and increases at higher g_{GABA}. F: Simulation of*

membrane currents (downward deflections) and membrane changes (upward deflections) upon a GABAergic (blue traces) and glutamatergic stimulation. Gray and light orange traces represent temporally shifted glutamatergic inputs, performed to differentiate the effects of conductance vs. depolarization effects. Note that the depolarization shift outlasts the conductance shift for both inputs. G: Influence of the timing between AMPA and GABA input on Δg_{AMPA}^{Thr} determined at 3 exemplary E_{GABA}. Note that the maximal inhibitory effect at hyperpolarizing (E_{GABA} = -55 mV) or pure shunting GABAergic inputs (E_{GABA} = -50.5 mV) were observed for synchronous AMPA inputs, while the excitatory influence of GABA at depolarized E_{GABA} of -43 mV was maximal for substantially delayed AMPA inputs. H: Quantification of E_{GABA}^{Thr} (dark blue) for different delays between GABA and AMPA inputs. Note that for AMPA inputs preceding GABA inputs E_{GABA}^{Thr} was close to the AP threshold, while for AMPA inputs lagging GABA inputs E_{GABA}^{Thr} approximated -50.5 mV. The light blue traces represent E_{GABA}^{Thr} determined for pure simulated GABAergic depolarizations which persistently results in a E_{GABA}^{Thr} close to -50.5 mV.

In the first set of experiments we simulated the effect of GABA pulses provided synchronously with AMPA inputs in a ball model (Fig. 4A) using a constant g_{GABA} of 2.37 nS. These experiments demonstrated that the co-stimulation of a GABAergic input can attenuate or enhance AP triggering upon glutamatergic stimulation, depending on E_{GABA} (Fig. 4A). As expected, such a GABA co-stimulation enhanced g_{AMPA}^{Thr} at hyperpolarized E_{GABA}, while smaller g_{AMPA}^{Thr} values were required at more depolarized E_{GABA} (Fig. 4B). From the intersection of this g_{AMPA}^{Thr} with the g_{AMPA}^{Thr} recorded in the absence of GABAergic inputs we determined that E_{GABA}^{Thr} amounted to −44.7 mV under this condition (Fig. 4B), which is considerable more negative than E_{Thr}^{ST} of −43.04 mV in the ball model. Additional experiments with different g_{GABA} values revealed that E_{GABA}^{Thr} depends on g_{GABA} (Fig. 4C-E). However, only at rather large g_{GABA} values E_{GABA}^{Thr}

approached toward values > −44 mV. At lower, physiologically more relevant g_{GABA} values E_{GABA}^{Thr} converges to a value of −44.9 mV (Fig. 4E). This observation indicates that E_{GABA}^{Thr} was consistently lower than E_{Thr}^{ST}, implying that GABAergic inputs are under these conditions more excitatory than expected from the difference between E_{GABA} and E_{AP}^{Thr}.

Is has already been proposed that the GABAergic depolarization outlasts the GABAergic currents and can add an additional excitatory drive to neurons [39]. Our simulations replicated this typical behavior, both GABAergic and glutamatergic membrane depolarization outlasted the time course of the respective currents (Fig. 4F). To investigate whether the systematic shift of E_{GABA}^{Thr} towards more hyperpolarized potentials was indeed caused by the differential impact of GABAergic conductance and GABAergic membrane depolarization on the AMPA-mediated excitation, we systematically advanced or delayed the time point of AMPA inputs (Fig. 4 F). These simulations revealed that, as expected, the strongest inhibitory effect of a GABAergic input for both hyperpolarizing (at E_{GABA} < RMP) and shunting inhibition (at E_{GABA} = RMP) was observed when it was synchronous to the glutamatergic input (Fig. 4G). In contrast, at more depolarized E_{GABA} the maximal excitatory effect occurred when the AMPA input was given about 60 ms after the GABA input (Fig. 4G, light trace), i.e. at a time point when the GABAergic conductance virtually ceased, but a considerable GABAergic depolarization persisted (Fig. 4F, blue traces). A systematic determination of E_{GABA}^{Thr} for different delays demonstrated that E_{GABA}^{Thr} was relatively stable around −43 mV for APMA inputs that preceded GABA inputs, and was thus close to E_{Thr}^{ST} (Fig. 4H). In contrast, with increasing delays of the glutamatergic inputs E_{GABA}^{Thr} converged to −50.5 mV, i.e. to the RMP determined by the reversal potential of the passive membrane conductance (Fig. 4H). In summary, these findings suggest (i) that at preceding AMPA inputs the influence of GABA on this glutamatergic input was dominated by the GABAergic conductance change and

thus converged to E_{Thr}^{ST} and (ii) that at delayed glutamatergic inputs the influence of GABA on this glutamatergic input was dominated by the GABAergic depolarization.

In the absence of a GABAergic conductance shift each depolarization above −50.5 mV should reduce the distance to the E_{AP}^{Thr} and should thus impose an excitatory effect. To verify this hypothesis, we recorded the GABAergic currents at different E_{GABA} and replayed these currents to the modelled neurons via I-clamp, thereby isolating the effect of the GABAergic depolarization from the conductance shift. Indeed, these simulations demonstrated that the effect of the pure GABAergic depolarization reversed at an E_{GABA} of −50.5 mV (Fig. 4H, light trace).

In summary these experiments demonstrated that the effect of a GABAergic stimulus on glutamatergic synaptic inputs cannot simply be predicted from the difference between E_{GABA} and the E_{AP}^{Thr} threshold, but that, depending on the temporal relation between GABAergic and glutamatergic inputs, E_{GABA} is substantially lower than E_{AP}^{Thr} and thus GABA acts more excitatory than expected from the E_{GABA} to E_{AP}^{Thr} relation.

In the next set of experiments, we evaluated how the spatial relation between GABAergic and glutamatergic inputs affects E_{GABA}^{Thr} in a ball-and-stick model. For these simulations, we systematically varied both, GABA and AMPA synapse along the dendrite, using 20 equidistant positions each (Fig. 5A), and stimulated both synapses.

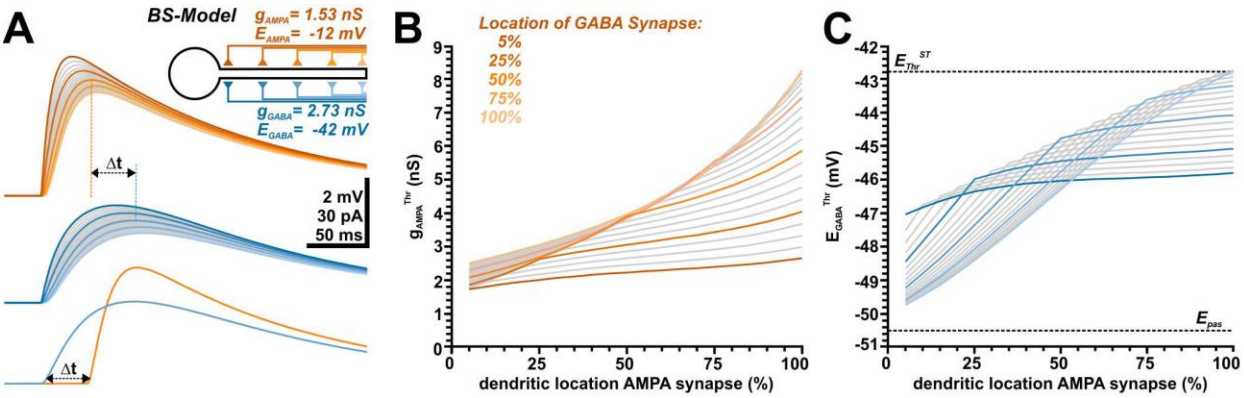

Figure 5. *Influence of the spatial relation between the AMPA receptor-dependent and the GABA receptor-dependent synaptic input on* g_{AMPA}^{Thr} *and* E_{GABA}^{Thr}*. A: Simulated voltage traces illustrating the membrane responses induced by AMPA synapses (orange traces) and by GABA synapses (blue traces) located at different dendritic locations. The colored traces represent synapses at 5%, 25%, 50%, 75% and 100% of the dendritic length, as color-coded in the schematic inset. Note the slower onset kinetics and delayed peak for distant dendritic synapses. The lower traces depict how the delay of GABA and AMPA was adjusted to obtain synchronous peak depolarizations. B: Effect of the dendritic location on* g_{AMPA}^{Thr} *simulated for 20 equidistant positions of the GABAergic synapse (*g_{GABA} *=7.89 nS;* E_{GABA} *= -44 mV). Each line represents the results for one GABA synapse position, the color code identifies every* 5^{th} *position as indicated. Note the shallow dependency of* Δg_{AMPA}^{Thr} *for proximal and the steep dependency for distal GABA synapses. C: Dependency of* E_{GABA}^{Thr} *on the dendritic positions of AMPA synapses, each line represents the results for one GABA synapse position, with shade coding as in B. Note the shallow location dependency with* E_{GABA}^{Thr} *around -46 mV for the proximal GABA synapses, while for distal GABA synapses a steep* E_{GABA}^{Thr} *profile between ca. -43 mV and -50 mV was observed.*

Simulations of single inputs revealed that the time course of the glutamatergic and GABAergic depolarizations critically depended on the dendritic location (Fig. 5A), which reflect spatial filtering [58]. To prevent that this temporal scattering affects the spatial analysis of GABA/AMPA relations, we determined the maximum of the depolarization in control sweeps performed before each run of the definite simulation for each combination of g_{AMPA}, AMPA location, E_{GABA}, and GABA location in the absence of an AP mechanism. For the definite simulation sweep the temporal relation between glutamatergic and GABAergic input was shifted such that peak depolarization of GABA and AMPA responses coincided (Fig. 5A).

To get an impression how a depolarizing GABAergic input at different locations influences g_{AMPA}^{Thr}, we first varied the position of a GABAergic synapse with a g_{GABA} of 7.89 nS and an E_{GABA} of −44 mV along the dendrite and determined g_{AMPA}^{Thr} for each of the 20 AMPA synapse along the dendrite (Fig. 5B). These simulations showed, as expected, that (i) g_{AMPA}^{Thr} increased with increasing dendritic distance, and (ii) that for a soma-near GABAergic synapse the excitatory effect of GABA was stronger than for distal dendritic locations, as indicated by the larger g_{AMPA}^{Thr} required for the distal GABA synapses (Fig. 5B). However, we could also demonstrate that (iii) the slope of the g_{AMPA}^{Thr} became shallower for AMPA inputs distal to the GABA inputs (Fig. 5B), indicating a strong non-linear influence of GABAergic inputs. To determine how the spatial relation between glutamatergic and GABAergic inputs affects E_{GABA}^{Thr} we subsequently varied E_{GABA} (at g_{GABA} of 7.89 nS) for all combinations of synaptic positions and determined when Δg_{AMPA}^{Thr} switches the direction (Fig. 5C). These simulations revealed a complex relation between these three parameters. If the GABAergic synapse was located in the proximal dendrite close to the soma (Fig. 5, dark trace) E_{GABA}^{Thr} was only weakly dependent on the site of the AMPA synapse and amounted to values between ca. −45 mV and −46 mV. If the GABA synapse was located more distally (Fig. 5, lighter trace) E_{GABA}^{Thr} showed a step dependency on the location of the AMPA synapse for all AMPA synapses located proximally to the GABA synapse, while the shallow dependency was maintained for the more distal synapses (Fig. 5C). Under this condition E_{GABA}^{Thr} approached −50 mV for proximal AMPA synapses, i.e. when both synapses were 950 µm apart and thus the GABAergic depolarization dominated over the more local shunting effect (see lightest blue trace in Fig. 5C). In contrast, for most distally located AMPA and GABA synapses, which represent spatially correlated inputs distant from the AP initiation zone, E_{GABA}^{Thr} approached E_{Thr}^{ST} (Fig. 5C).

In summary, these results demonstrate that both, the spatial relation between GABAergic and glutamatergic synapses as well as the location of the GABA synapse influences E_{GABA}^{Thr}. However, only for spatially correlated inputs at distal dendrites E_{GABA}^{Thr} was close to the E_{AP}^{Thr}. With increasing distance between both synapses and with a closer approximation of the GABA synapse to the soma, E_{GABA}^{Thr} was shifted to more negative values, again indicating that GABA mediates a more prominent excitatory action than expected from the difference between E_{GABA} and E_{AP}^{Thr}.

2.4. Effect of tonic GABAergic inputs on glutamatergic excitation

GABA influences neuronal excitability not only via synaptic inputs, but also extrasynaptic, tonic GABAergic currents substantially contribute to the GABAergic effects [59,60] and can mediate even excitation during development [45]. Therefore, we next analyzed how a tonic GABAergic conductance (g_{GABA}^{tonic}) influences g_{AMPA}^{Thr} and E_{GABA}^{Thr} in a ball model (Fig. 6A), using a g_{GABA}^{tonic} between 8.75 fS/cm^2 and 8.75 nS/cm^2, corresponding to values from 1/100 to 10000 times of the experimentally determined tonic GABA conductance of 0.875 pS/cm^2 [52].

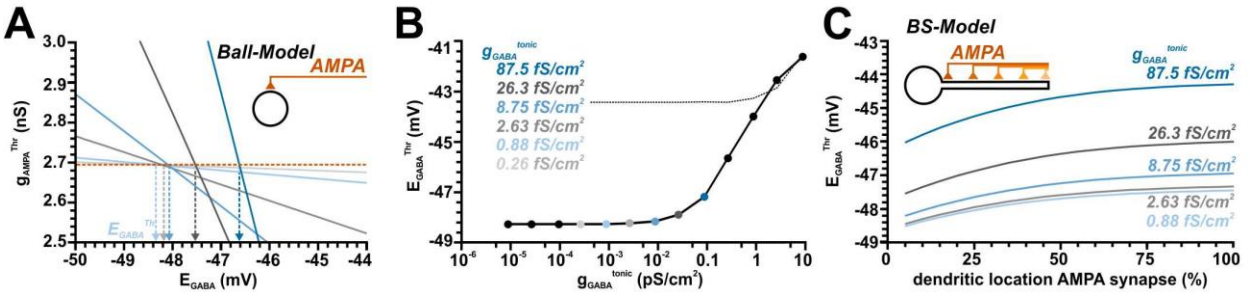

Figure 6. *Influence of tonic GABAergic conductances on the AMPA receptor-dependent excitability in a simple ball and a ball-and-stick model. A: Plot of g_{GABA}^{Thr} at different E_{GABA}. The differently shaded lines represent different tonic g_{GABA} values as indicated in B. The increased slope of the curves with higher g_{GABA}^{tonic} illustrates the higher inhibitory effect under*

this conditions. From the intersection of the plots with the g_{GABA}^{Thr} value obtained in the absence of tonic GABA (orange line) the E_{GABA}^{Thr} values were determined. B: Plot of E_{GABA}^{Thr} determined at different g_{GABA}^{tonic}. The dashed line represents E_{Thr}^{ST}. Note that E_{GABA}^{Thr} is negative to E_{Thr}^{ST} for g_{GABA}^{tonic} < ca 3 pS/cm^2. C: Influence of different dendritic locations of AMPA synapses in a ball-and-stick model on the AMPA receptor-dependent excitability determined for different g_{GABA}^{tonic}. Note the substantial shift of E_{GABA}^{Thr} to positive values with more distant AMPA synapses and the systematic depolarized shift with increasing g_{GABA}^{tonic}.

These experiments demonstrated, that g_{GABA}^{tonic} can attenuate or enhance AP induction by AMPA synapses, depending on E_{GABA}. As expected, the slope of the GABAergic influence increased with g_{GABA}^{tonic} (Fig. 6A). And as expected, tonic GABAergic conductance enhanced g_{AMPA}^{Thr} at hyperpolarized E_{GABA}, while smaller g_{AMPA}^{Thr} values were required at more depolarized E_{GABA} (Fig. 6A). From the intersection of these g_{AMPA}^{Thr} with the basal g_{AMPA}^{Thr} (obtained in the absence of tonic GABA), E_{GABA}^{Thr} was determined (Fig. 6B). Notably, these E_{GABA}^{Thr} were rather constant at ca. −48.3 mV within a wide range of g_{GABA}^{tonic}, spanning from 0.001 to ca. 10 times the experimentally determined g_{GABA}^{tonic} value. Only at very high g_{GABA}^{tonic} of > 100 fS/cm^2 E_{GABA}^{Thr} approached E_{Thr}^{ST} (which under these conditions was shifted to positive values due to the massively enhanced total membrane conductance). In summary, these results indicate that tonic GABAergic conductances can mediate an excitatory effect even if E_{GABA} was substantially negative to E_{AP}^{Thr}.

Finally, we investigated how the E_{GABA} of g_{GABA}^{tonic} affects the excitation generated by AMPA synapses located along the dendrite in a ball-and-stick model (Fig. 6C). These simulations revealed (i) that E_{GABA}^{Thr} was systematically shifted to positive values (closer to E_{AP}^{Thr}) for distal AMPA synapses and (ii) that E_{GABA}^{Thr} was also more positive (and thus closer to E_{AP}^{Thr}) for larger g_{GABA}^{tonic} at all dendritic positions (Fig. 6C). These observations suggest that a tonic GABAergic

464 conductance mediates an excitatory effect even at E_{GABA} that is substantially negative to E_{AP}^{Thr},

465 but that an inhibitory effect of tonic GABAergic conductance is higher at distal AMPA-mediated

466 inputs.

3. Discussion

Experimental findings indicate that $[Cl^-]_i$ and $[HCO_3^-]_i$ are dynamically shifted during early brain development, upon massive GABAergic activity and after pathophysiological insults [10,15,61]. Thus it became evident that GABA can have depolarizing actions [8,13] and this raised the question under which conditions the activation of $GABA_A$ receptors can mediate an excitatory effect. Theoretical considerations suggested that $GABA_A$ receptor activation permits an inhibitory effect as long as E_{GABA} was below E_{Thr}^{AP} [35,36]. However, this consideration just reflects a quasi one-dimensional situation and ignores the temporal and spatial components of GABAergic membrane responses as well as the restriction imposed by the passive membrane properties within more complex neuronal topologies [37–39]. Because the exact role of GABA on the excitation/inhibition threshold is therefore hard to predict from such theoretical assumptions, we performed a detailed in-silico study using a simple neuronal topology and distinct spatiotemporal relations between GABAergic and glutamatergic inputs to evaluate at which E_{GABA} values the net GABA effect switches from inhibitory to excitatory. In these simulations we were able to demonstrate that (i) for GABAergic synapses located close to the AP initiation zone (AIP) the difference between E_{GABA} and E_{AP}^{Thr} indeed reliably predicts whether GABA has an excitatory or inhibitory action. (ii) The threshold GABA reversal potential (E_{GABA}^{Thr}) was in this case close to the E_{AP}^{Thr} defined by the maximal subthreshold current injection (E_{Thr}^{ST}). (iii) E_{GABA}^{Thr} was systematically shifted to positive values with increasing distance between the GABA synapse and the AIP. (iv) An excitatory effect of GABA inputs on synchronous AMPA mediated inputs was observed when E_{GABA} was above −44.9 mV, and thus consistently hyperpolarized to E_{AP}^{Thr}. (v) E_{GABA}^{Thr} critically depends on the temporal relation between GABA and AMPA inputs, with a striking excitatory effect on AMPA-mediated inputs appearing after the GABA input. (vi) The spatial relation between GABAergic and AMPA-mediated inputs critically influences E_{GABA}^{Thr},

with E_{GABA}^{Thr} systematically being shifted to values negative to E_{AP}^{Thr} for AMPA synapses located proximally to the GABA input. (vii) For tonic GABAergic conductances, E_{GABA}^{Thr} was systematically negative to E_{AP}^{Thr} over a wide range of g_{GABA}^{tonic} values spanning the physiological range. In summary, these results demonstrate that only for very restricted conditions the GABAergic effects switch from excitation to inhibition when E_{GABA} was at E_{AP}^{Thr}. Under several physiologically relevant conditions, E_{GABA}^{Thr} was negative to E_{AP}^{Thr}, suggesting that GABA can mediate excitatory effects already under these conditions.

It is important to note that in the present study we considered only E_{GABA} as the relevant parameter, which in reality depends not only on $[Cl^-]_i$ but also on $[HCO_3^-]_i$ [6]. We have chosen this approach to (i) ease the computational load, (ii) because the consideration of two independent variables makes the interpretation of the results more complicated, and (iii) because the relative HCO_3^- conductance of $GABA_A$ receptors differs between distinct neuronal subpopulations [6,62,63]. Differences in intracellular fixed charges can also slightly influence the relation between $[Cl^-]_i$, E_{Cl} and the GABAergic driving force [64,65]. In addition, we did not consider that functionally relevant somato-dendritic $[Cl^-]_i$ gradients exists in neurons [11,66] and that GABAergic synaptic activity, alone or correlated to glutamatergic inputs, considerably alters E_{GABA} [49,52,61,67–70]. All of these properties will complicate the prediction of GABAergic response direction, however, for any interpretation of the functional consequences of temporal and spatially dynamic $[Cl^-]_i$ (and $[HCO_3^-]_i$) gradients, it will be necessary to obtain a major framework to understand how the GABAergic response direction depends on the relation between E_{GABA}, E_{AP}^{Thr} and spatiotemporal synaptic properties.

The first major result of this in-silico study was the observation that E_{GABA}^{Thr} determined for the GABAergic effect on AMPA-mediated inputs was in many cases considerably negative to E_{AP}^{Thr}, in contrast to the initial theoretical consideration [35,36]. In our experiment we were also able to

provide a mechanistic explanation for this observation. First, by using a current-clamp approach we could replicate that the GABAergic depolarization, when isolated from the GABAergic conductance shift, acted excitatory whenever the peak GABAergic depolarization was positive to the RMP, resulting in an E_{GABA}^{Thr} of −50.5 mV. This stringent excitatory effect can be easily explained by the fact that in the absence of conductance changes each depolarization brings E_m closer to E_{AP}^{Thr}. Next, we could demonstrate, by providing AMPA-inputs with a defined advance or delay to the GABAergic inputs, a clear bimodal effect of depolarizing GABA responses. In all cases in which the AMPA inputs preceded the GABA input E_{GABA}^{Thr} was close to E_{AP}^{Thr} (Fig. 4H). Under this condition the AP initiation was under the control of the subsequent GABAergic conductance shift. And under this condition, the $GABA_A$ receptor will mediate an inward current, corresponding to a putative excitatory effect, as long as E_{GABA} was positive to E_m, Thereby, an excitatory effect was induced only if E_{GABA} was above E_{AP}^{Thr}. However, if the AMPA-mediated inputs occurred after the GABAergic inputs, E_{GABA}^{Thr} was systematically shifted to more negative values approximating the RMP of −50.5 mV. This effect can be attributed to the fact that the GABAergic depolarization outlasts the GABAergic conductance shift. Thus, under these conditions the depolarization progressively dominates the effect of GABA, leading to a gradual shift in E_{GABA}^{Thr} towards more negative potentials. If the GABAergic conductance can be neglected, each depolarizing shift, i.e. each membrane change depolarized to RMP, contributed to the excitation, leading again to an E_{GABA}^{Thr} of −50.5 mV. The impact of the temporal profile of GABAergic conductance change vs. GABAergic depolarization on neuronal excitability has already been experimentally addressed in hypothalamic [39] and neocortical [40] neurons, where the initial phase of a GABA response prevented AP initiation, whereas at later time points of the GABAergic responses AP initiation was facilitated. Despite this clear latency-dependent effect, the reciprocal actions of a depolarization-induced facilitation and a conductance-induced shunting

inhibition can also explain why E_{GABA}^{Thr} for synaptic inputs was neither at RMP, which would be the case if only the membrane potential shift was relevant, nor at E_{Thr}^{AP}, which would be the case if E_m was only dependent on the actual GABAergic conductance.

In immature neurons, with their slow membrane time constants [71,72], the membrane responses are most probably prone to outlast the membrane conductance for both glutamatergic and GABAergic synaptic inputs. On the other hand, this effect of a prolonged membrane time constant in immature neurons may be partially compensated by the fact, that immature synaptic GABAergic currents show significantly longer decay time constants [72], thereby prolonging the interval in which the shunting inhibitory effects contributes to E_{GABA}^{Thr}. Another important functional consequence of our results is that the timing between GABAergic and glutamatergic inputs critically determines E_{GABA}^{Thr}. In this respect classical feedforward as well as recurrent inhibition, with its short latency to excitatory inputs [73], will impose a rather strict inhibition even at depolarizing GABAergic conditions as long as E_{GABA} is maintained below E_{Thr}^{AP}. Thus this kind of inhibitory control would be rather stable upon activity dependent shifts in E_{GABA} [49,61,67,68,74]. On the other hand, for GABAergic inputs that are not temporally correlated with the excitatory inputs, e.g. during blanket inhibition, it must be considered that E_{GABA}^{Thr} can be negative to E_{AP}^{Thr}, and thus may mediate a less stable inhibition that is more sensitive to ionic plasticity.

The second major result of this in-silico study was the observation, that the spatial relation between GABAergic and AMPA inputs also critically affects E_{GABA}^{Thr}. As expected, our simulation revealed that the inhibitory effect, as quantified by Δg_{AMPA}^{Thr}, of proximal GABAergic synapses are stronger than that of distally located ones. The Δg_{AMPA}^{Thr} values were substantially larger for AMPA synapses located distally to the GABA synapse, indicating that a GABA input can shunt EPSPs from distally located excitatory synapses, as suggested from in-vitro and in-silico

experiments [40]. For proximally located GABA synapses we could observe that E_{GABA} showed only little dependency on the location of the AMPA-mediated inputs. In these cases, $E_{GABA}{}^{Thr}$ amounted to ca. −46 mV, suggesting that both, shunting and depolarizing effects contribute to the impact of GABA on the excitability. In contrast, we observed for distally located GABA synapses a strong dependency of the location of AMPA-mediated inputs on $E_{GABA}{}^{Thr}$. For such distal GABA synapse locations a negative $E_{GABA}{}^{Thr}$ close to −50 mV was observed at proximal AMPA synapses, which reflects the fact that with this configuration only the electrotonically propagating GABAergic depolarization has an effective influence on the AMPA-mediated depolarization, while the GABAergic conductance shift acts more locally. For co-localized GABA and AMPA synapses at the distal end of the dendrite $E_{GABA}{}^{Thr}$ approximated $E_{AP}{}^{Thr}$ at ca. −43 mV, indicating that here the effect of GABA was mediated mainly by membrane shunting. Intriguingly the "slope" of $E_{GABA}{}^{Thr}$ was steeper for AMPA synapses in the dendritic segment proximal to the GABA synapse. The slope became shallower for the segment distal from the GABA synapse. This observation indicates that for all AMPA synapses distal to the GABA synapse a substantial fraction of the synaptic currents were shunted by the GABAergic conductance before they can affect AP initiation in the soma. In contrast, for all AMPA synapses located proximal to the GABA synapse the shunting effect was diminished with increasing distance between both synapses, whereas the electrotonically propagating depolarization maintained a more stable excitatory influence and thereby shifted $E_{GABA}{}^{Thr}$ towards the RMP. Thus the results of our experiments suggest an additional mechanism that contribute the putative excitatory GABAergic effect of dendritic GABA inputs [40], in addition to the existence of stable or dynamic somato-dendritic $[Cl^-]_i$ gradients [75,76].

These in-silico observations indicate that perisomatic inhibition, which is the dominant form for the classical feedback and feedforward inhibition mediated by parvalbumin-positive interneurons

587 [77,78], can maintain a stable inhibitory effect regardless of the site of glutamatergic inputs and
588 ionic plasticity. On the other hand, the impact of GABAergic synapses located in the dendritic
589 periphery, e.g. by the hippocampal O-LM interneurons [79] or neocortical Martinotti interneurons
590 [80], will critically depend on the location of the excitatory glutamatergic inputs and can putatively
591 mediate an excitatory impact on AMPA synapses close to the soma at slightly depolarizing E_{GABA}.

592 In addition, our results indicate that for small to moderate tonic GABAergic conductance $E_{GABA}{}^{Thr}$
593 was systematically more negative than $E_{AP}{}^{Thr}$, which suggests that even at rather moderate
594 depolarizations tonic GABAergic currents can mediate an excitatory effect. Only at higher
595 $g_{GABA}{}^{tonic}$ the $E_{GABA}{}^{Thr}$ approaches $E_{AP}{}^{Thr}$. The results of this simulation replicate the findings of a
596 previous in-vitro study, that demonstrated excitatory effects of depolarizing tonic GABAergic
597 responses at low conductances, whereas at higher conductances a stable inhibition was imposed
598 [81]. Our results are also in line with the excitatory effects of extrasynaptic $GABA_A$ receptors in
599 the immature hippocampus [45]. In our simulations $E_{GABA}{}^{Thr}$ remained stable at about −48.3 mV
600 for $g_{GABA}{}^{tonic}$ smaller than ca. 10^{-2} pS/cm^2, which is close to the passive membrane conductance
601 g_{pas} of 0.0128 pS/cm^2. We assume that below this value the shunting effects caused by $g_{GABA}{}^{tonic}$
602 were negligible to the background conductance g_{pas} and thus did not considerably contribute to the
603 shunting of EPSCs. Only if $g_{GABA}{}^{tonic}$ exceeded g_{pas} a relevant additional inhibitory component was
604 imposed by the GABAergic conductances and thus $E_{GABA}{}^{Thr}$ converged towards $E_{AP}{}^{Thr}$.

605 Another conclusion that could be drawn from our study is that some attention should be taken to
606 the method used to detect the AP threshold. Obviously there is, despite the frequent use of this
607 descriptive parameter, no consensus on the definition of AP threshold [42]. Therefore, we used in
608 this in-silico study four different, established methods for $E_{AP}{}^{Thr}$ detection. Our in-silico
609 experiments demonstrated that the AP threshold value determined from a fixed threshold of dV/dt
610 [44,50], from the first positive peak in d^3V/dt^3 [51], and from linear regression of the AP upstroke

611 [43] were comparable at potentials of ca. −34 mV to −37 mV. In contrast, substantially negative
612 values of −43 mV were determined if E_{AP}^{Thr} was defined as the maximal potential that did not
613 result in AP triggering (E_{Thr}^{ST}). The difference in the results of these methods can be easily
614 explained by the fact that E_{Thr}^{ST} represents a quasi-stationary value (dV/dt close to 0) that is just
615 insufficient to trigger the entry to the Hodgkin cycle. On the other hand, the first three E_{AP}^{Thr} values
616 represent distinct states during the dynamic events in the initial AP phase. The fact that in our
617 simulations E_{GABA}^{Thr} for only GABAergic inputs indeed approximated E_{Thr}^{ST} can be related to the
618 fact that the excitation threshold for GABAergic inputs was also determined under quasi-stationary
619 conditions. For the influence of GABA on synaptic AMPA-mediated inputs the excitation
620 threshold was determined in the interval between the onset of the GABA inputs and the duration
621 at which 63% of the peak depolarization was obtained. Thus, for the relevant traces that
622 distinguished between subthreshold and suprathreshold AMPA inputs, dV/dt was considerable
623 small and thus the AP threshold was also determined under quasi stationary conditions. Under
624 physiological conditions random fluctuation in E_m will most probably limit the difference between
625 E_{Thr}^{dVdt}, E_{Thr}^{d3}, E_{Thr}^{IS}, and E_{Thr}^{ST}. In any way, while addition of membrane noise to the in-silico
626 models and/or a different methodological definition of the excitation threshold for GABA- and
627 AMPA-mediated inputs would probably change the absolute values for E_{GABA}^{Thr} and E_{AP}^{Thr}, it
628 would not substantially interfere with the main observation of this study, that E_{GABA}^{Thr} is for many
629 physiologically relevant situations negative to E_{AP}^{Thr}.

630 In conclusion, this simulation indicates that, in addition to the influence of short-term and long-
631 term ionic plasticity, the uneven distribution of $[Cl^-]_i$ gradients within individual cells and the
632 effects of tonic and phasic inhibition [10,11,61,67], the observed spatial and temporal constraints
633 on the E_{GABA} to E_{AP}^{Thr} relation imposes another level of complexity to the dynamic properties of
634 GABAergic inhibition/excitation. While on one hand our results support the textbook knowledge

635 that GABA mediates a stable inhibition as long as hyperpolarizing membrane responses are evoked
636 (or $[Cl^-]_i$ is sufficiently low), on the other hand the altered $[Cl^-]_i$ homeostasis in early development
637 and several neurological conditions like trauma, stroke or epilepsy [11,12,30,31], can impact the
638 level of inhibitory control already upon moderate $[Cl^-]_i$ changes in a complex way.

4. Materials and Methods

4.1. Electrophysiological procedures

4.1.1. Slice preparation

All experiments were conducted in accordance with EU directive 86/609/EEC for the use of animals in research and the NIH Guide for the Care and Use of Laboratory Animals, and were approved by the local ethical committee (Landesuntersuchungsanstalt RLP, Koblenz, Germany). We made all efforts to minimize the number of animals and their suffering. Newborn pups of postnatal days [P] 4-7 were obtained from time pregnant C57Bl/6 mice (Janvier Labs, Saint Berthevin, France) housed in the local animal facility at 12/12 day/night cycle and ad libitum access to food and water. The mouse pups were decapitated in deep enflurane (Ethrane, Abbot Laboratories, Wiesbaden, Germany) anaesthesia, their brains were quickly removed and immersed for 2-3 min in ice-cold standard artificial cerebrospinal fluid (ACSF, 125 mM NaCl, 25 mM $NaHCO_3$, 1.25 mM NaH_2PO_5, 1 mM $MgCl_2$, 2 mM $CaCl_2$, 2.5 mM KCl, 10 mM glucose, equilibrated with 95% O_2 / 5 % CO_2, osmolarity 306 mOsm). Four hundred µm thick horizontal slices including the hippocampus were cut on a vibratome (Microm HM 650 V, Thermo Fischer Scientific, Schwerte, Germany) and subsequently stored in an incubation chamber filled with oxygenated ACSF at room temperature for at least 1h before they were transferred to the recording chamber.

4.1.2 Patch-clamp recordings

Whole-cell patch-clamp recordings were performed at 31 ± 1 °C in a submerged-type recording chamber attached to the fixed stage of a microscope (BX51 WI, Olympus). Pyramidal neurons in the stratum pyramidale of the CA3 region were identified by their location and morphological appearance in infrared differential interference contrast image. Patch-pipettes (5-12 MΩ) were pulled from

662 borosilicate glass capillaries (2.0 mm outside, 1.16 mm inside diameter, Science Products, Hofheim,
663 Germany) on a vertical puller (PP-830, Narishige) and filled with the pipette solutions (86 mM K-
664 gluconate, 44 mM KCl, 4 mM NaCl, 1 mM $CaCl_2$, 11 mM EGTA, 10 mM K-HEPES, 2 mM Mg2-
665 ATP, 0.5 mM Na-GTP, pH adjusted to 7.4 with KOH and osmolarity to 306 mOsm with sucrose). In
666 few experiments 40 mM KCl were replaced with 40 mM K-gluconate. Signals were recorded with a
667 discontinuous voltage-clamp/current-clamp amplifier (SEC05L, NPI, Tamm, Germany), low-pass
668 filtered at 3 kHz and stored and analyzed using an ITC-1600 AD/DA board (HEKA) and TIDA
669 software. All voltages were corrected post-hoc for liquid junction potentials of -8 mV for a [Cl^-] of 10
670 mM and -5 mV for 50 mM [20]. Input resistance and capacitance were determined from a series of
671 hyperpolarizing current steps. Action potentials (AP) were induced by a series of depolarizing current
672 steps. For averaging of AP wave forms the first AP from traces that showed a series of APs were used.

673

674 **4.2. Compartmental modeling**

675 The compartmental modeling was performed using the NEURON environment (neuron.yale.edu).
676 The source code of models and stimulation files used in the present paper can be found in
677 ModelDB (http://modeldb.yale.edu/267062; reviewer password is “GABA”). For compartmental
678 modelling we used either a simple ball (soma diameter = 43 µm) or a ball and stick model (soma
679 with d=43 µm, linear dendrite with l=1000 µm, diameter 1 µm, and 301 nodes). In both models a
680 passive conductance (g_{pas}) with a density of $1.28*10^{-5}$ nS/cm^2 and a reversal potential (E_{pas}) of
681 −50.5 mV was distributed, which resulted for the ball-and-stick model in passive membrane
682 properties that were comparable to the properties of recorded pyramidal CA3 neurons.

683 Because it was not possible to generate a reasonable sharp AP onset with a standard Hodgkin-
684 Huxley (HH) model and since we are particularly interested in the AP threshold properties, we

heuristically developed a modified Markov model, massively simplified from published Markov models [82,83] to simulate the AP with a considerably precision. For this modified Markov model we consider only 3 different states for the Na^+ channels [84]:

Na_o = *open state*

Na_i = *inactive state, closed*

Na_c = *closed state, activatable*

We restricted transitions between these states to $Na_c \rightarrow Na_o$, $Na_o \rightarrow Na_i$, $Na_i \rightarrow Na_c$, $Na_c \rightarrow Na_i$.

The transition rate $Na_c \rightarrow Na_o$ is only voltage dependent as described by a Bolzmann function:

$$\frac{dV}{dt} = Q_{10} \times \frac{G_{c\rightarrow o}^{Na}}{\left(1 + e^{\frac{(V_t - V_{c\rightarrow o}^{Na})}{k_{c\rightarrow o}^{Na}}}\right)}$$

The transition $Na_o \rightarrow Na_i$ is simulated by a voltage dependent kinetic rate described by a Bolzmann equation with is operational after a defined delay period plus a constant voltage-independent term

$$\frac{dV}{dt} = Q_{10} \times \frac{G_{o\rightarrow i}^{Na}}{\left(1 + e^{\frac{(V_{t\Delta} - V_{o\rightarrow i}^{Na})}{k_{o\rightarrow i}^{Na}}}\right)} + c_{o\rightarrow i}^{dec}$$

The transition rates $Na_c \rightarrow Na_i$ and $Na_i \rightarrow Na_c$ are described again by simple Bolzmann functions as follows:

$$\frac{dV}{dt} = Q_{10} \times \frac{G_{c\rightarrow i}^{Na}}{\left(1 + e^{\frac{(V_t - V_{c\rightarrow i}^{Na})}{k_{c\rightarrow i}^{Na}}}\right)} \; and \; \frac{dV}{dt} = Q_{10} \times \frac{G_{i\rightarrow c}^{Na}}{\left(1 + e^{\frac{(V_t - V_{i\rightarrow c}^{Na})}{k_{i\rightarrow c}^{Na}}}\right)}$$

In addition, we implemented a simple two state modified Markov model for the delayed rectifier K^+ current, with the $K_c \rightarrow K_o$ transition rate described by a Bolzmann equation with an operational delay period as follows:

$$\frac{dV}{dt} = Q_{10} \times \frac{G^K_{c\rightarrow o}}{\left(1 + e^{\frac{(V_{t\Delta} - V^K_{c\rightarrow o})}{k^K_{c\rightarrow o}}}\right)}$$

And the $K_o \rightarrow K_c$ transition rate described by a Bolzmann equation with an operational delay period:

$$\frac{dV}{dt} = Q_{10} \times \frac{G^K_{o\rightarrow c}}{\left(1 + e^{\frac{(V_{t\Delta} - V^K_{o\rightarrow c})}{k^K_{o\rightarrow c}}}\right)}$$

All states for the Na^+ and K^+ channels are normalized at each iteration step as follows:

$$Na_o + Na_i + Na_c = 1 \text{ and } K_o + K_c = 1$$

The Na^+ current was given according to Ohms law as:

$$I_{Na}(t) = g_{Na} * Na_o(t) * (v(t)-E_{Na})$$

And the K^+ current was as:

$$I_K(t) = g_K * K_o(t) * (v(t)-E_K)$$

All parameters were optimized by stepwise approximation to obtain a sufficient fit to the average experimentally determined AP trace, which was quantified by minimizing the root of the summarized squared errors according to the following error weight function:

$$Error = 10 \times \sqrt{\left(E^{d3}_{Thr}\right)^2} + 3 \times \sqrt{(v^{max}_{rise})^2} + \sqrt{\left(v^{max}_{decay}\right)^2} + \sqrt{\left(d_{1/2}\right)^2} + \sqrt{\left(E^{Peak}_{AP}\right)^2}$$

This error function was used with the rationale to put special emphasise for the fitting routine to the dynamic properties at $E_{AP}{}^{Thr}$. The used parameters are given in Table 2.

718 AMPA synapses were modeled by an Exp2Syn point process using a reversal potential of -12 mV,
719 a tau1 value of 0.1 ms and a tau2 value of 11 ms, in accordance with the experimentally determined
720 value [49]. GABA synapses were modeled by an Exp2Syn point process using a tau1 value of 0.1
721 ms and a tau2 value of 37 ms, in accordance with the experimentally determined value [49]. The
722 reversal potential of the GABAergic synapses was the main variable of interest in these
723 simulations. For tonic GABAergic currents a constant membrane conductance was distributed over
724 all membrane with conductance densities and reversal potentials as given in the results part.

725 For the determination of g_{GABA}^{Thr} we used an iterative approach where g_{GABA} was first increased
726 by 1 nS steps until an AP was induced within an interval of 800 ms after the GABA input.
727 Subsequently g_{GABA} was decreased by 0.33 nS steps until the AP vanished, followed again by an
728 increase in g_{GAB}A by 0.1 pS until the AP reappeared. This alternating sequence was repeated 6
729 times using a g_{GABA} of 1/10 for each subsequent round. In these experiments E_{AP}^{Thr} was defined
730 as the peak voltage of the last subthreshold sweep.

731 A similar approach was also used to determine g_{AMPA}^{Thr}. Here g_{AMPA} was initially increased by
732 0.01 nS steps until an AP was induced. The analysis interval was in all sweeps set to the interval
733 between stimulus onset and the time point when the AMPA-mediated depolarization, determined
734 in the absence of an AP mechanism, decreased to 63% of the peak amplitude. Subsequent g_{AMPA}
735 was decreased by 3.3 pS until the AP disappears, followed by 6 rounds of alternating
736 increasing/decreasing g_{AMPA} steps, with g_{AMPA} step values decreasing by 1/10 for each round.

737

738 **Author Contributions:** Conceptualization: WK; Electrophysiological investigation: AL, Formal

739 analysis, AL and WK; Modeling: WK: Writing WK, AL, and HJL.

740

741 **Financial disclosure statement:** This research was funded by grants of the Deutsche
742 Forschungsgemeinschaft to WK (KI-835/3) and to HJL (CRC 1080, A01).

743

744 **Conflicts of Interest:** The authors declare no conflict of interest

745

746

References:

1. Mody I, Pearce RA. Diversity of inhibitory neurotransmission through GABA(A) receptors. Trends Neurosci. 2004;27: 569–575.

2. Whittington MA, Traub RD. Interneuron Diversity series: Inhibitory interneurons and network oscillations in vitro. Trends Neurosci. 2003; 26:676–682. doi:10.1016/j.tins.2003.09.016

3. Gabernet L, Jadhav SP, Feldman DE, Carandini M, Scanziani M. Somatosensory integration controlled by dynamic thalamocortical feed-forward inhibition. Neuron. 2005; 48:315-327. doi:10.1016/j.neuron.2005.09.022

4. Swanson OK, Maffei A. From hiring to firing: Activation of inhibitory neurons and their recruitment in behavior. Front Mol Neurosci. 2019;12: 1–9. doi:10.3389/fnmol.2019.00168

5. Ulrich D, Bettler B. GABAB receptors: synaptic functions and mechanisms of diversity. Curr Opin Neurobiol 2007; 17:298-303. doi:10.1016/j.conb.2007.04.001

6. Farrant M, Kaila K. The cellular, molecular and ionic basis of GABA(A) receptor signalling. ProgBrain Res. 2007;160: 59–87.

7. Mueller AL, Chesnut RM, Schwartzkroin PA. Actions of GABA in developing rabbit hippocampus: an in vitro study. Neurosci Lett. 1983; 39:193-198. doi:10.1016/0304-3940(83)90076-9

8. Ben-Ari Y, Cherubini E, Corradetti R, Gaiarsa J-L. Giant synaptic potentials in immature rat CA3 hippocampal neurones. J Physiol. 1989;416: 303–325.

9. Luhmann HJ, Prince DA. Postnatal maturation of the GABAergic system in rat neocortex. J Neurophysiol. 1991; 65:247-263. doi:10.1152/jn.1991.65.2.247

10. Blaesse P, Airaksinen MS, Rivera C, Kaila K. Cation-chloride cotransporters and neuronal function. Neuron. 2009;61: 820–838.

11. Kaila K, Price TJ, Payne JA, Puskarjov M, Voipio J. Cation-chloride cotransporters in neuronal development, plasticity and disease. Nat Rev Neurosci. 2014;15: 637–654. doi:10.1038/nrn3819

12. Watanabe M, Fukuda A. Development and regulation of chloride homeostasis in the central nervous system. Front Cell Neurosci. 2015; 9:371. doi:10.3389/fncel.2015.00371

13. Ben Ari Y, Woodin MA, Sernagor E, Cancedda L, Vinay L, Rivera C, et al. Refuting the challenges of the developmental shift of polarity of GABA actions: GABA more exciting than ever! Front Cell Neurosci. 2012;6:35.

14. Huebner CA, Holthoff K. Anion transport and GABA signaling. Front Cell Neurosci. 2013;7:177.

15. Kirmse K, Hübner CA, Isbrandt D, Witte OW, Holthoff K. GABAergic Transmission during Brain Development: Multiple Effects at Multiple Stages. Neuroscientist. 2018; 24:36-51. doi:10.1177/1073858417701382

16. Rivera C, Voipio J, Payne JA, Ruusuvuori E, Lahtinen H, Lamsa K, et al. The K+/Cl- co-transporter KCC2 renders GABA hyperpolarizing during neuronal maturation. Nature. 1999;397: 251–255.

17. Rohrbough J, Spitzer NC. Regulation of intracellular Cl- levels by Na(+)-dependent Cl- cotransport distinguishes depolarizing from hyperpolarizing GABAA receptor-mediated responses in spinal neurons. J Neurosci. 1996;16: 82–91.

18. Plotkin MD, Snyder EY, Hebert SC, Delpire E. Expression of the Na-K-2Cl cotransporter is developmentally regulated in postnatal rat brains: A possible mechanism underlying GABA's excitatory role in immature brain. J Neurobiol. 1997;33: 781–795.

19. Yamada J, Okabe A, Toyoda H, Kilb W, Luhmann HJ, Fukuda A. Cl- uptake promoting depolarizing GABA actions in immature rat neocortical neurones is mediated by NKCC1. J Physiol. 2004; 557:829-841. doi:10.1113/jphysiol.2004.062471

20. Achilles K, Okabe A, Ikeda M, Shimizu-Okabe C, Yamada J, Fukuda A, et al. Kinetic properties of Cl- uptake mediated by Na +-dependent K+-2Cl- cotransport in immature rat neocortical neurons. J Neurosci. 2007;27: 8616-8627. doi:10.1523/JNEUROSCI.5041-06.2007

21. Virtanen MA, Uvarov P, Hübner CA, Kaila K. NKCC1, an Elusive Molecular Target in Brain Development: Making Sense of the Existing Data. Cells. 2020;9: 1–20. doi:10.3390/cells9122607

22. Le Magueresse C, Monyer H. GABAergic Interneurons Shape the Functional Maturation of the Cortex. Neuron. 2013;77: 388–405. doi:10.1016/j.neuron.2013.01.011

23. Luhmann HJ, Kirischuk S, Sinning A, Kilb W. Early GABAergic circuitry in the cerebral cortex. Curr Opin Neurobiol. 2014;26:72-78. doi:10.1016/j.conb.2013.12.014

24. LoTurco JJ, Owens DF, Heath MJS, Davis MBE, Kriegstein AR. GABA and glutamate depolarize cortical progenitor cells and inhibit DNA synthesis. Neuron. 1995; 15:1287-1298. doi:10.1016/0896-6273(95)90008-X

25. Blanquie O, Liebmann L, Hübner CA, Luhmann HJ, Sinning A. NKCC1-Mediated GABAergic Signaling Promotes Postnatal Cell Death in Neocortical Cajal-Retzius Cells. Cereb Cortex. 2017;27: 1644–1659. doi:10.1093/cercor/bhw004

26. Inada H, Watanabe M, Uchida T, Ishibashi H, Wake H, Nemoto T, et al. GABA regulates the multidirectional tangential migration of GABAergic interneurons in living neonatal mice. PLoS One. 2011; 6:e27048. doi:10.1371/journal.pone.0027048

27. Sernagor E, Chabrol F, Bony G, Cancedda L. Gabaergic control of neurite outgrowth and remodeling during development and adult neurogenesis: General rules and differences in diverse systems. Front Cell Neurosci. 2010;4: 11. doi:10.3389/fncel.2010.00011

28. Deidda G, Allegra M, Cerri C, Naskar S, Bony G, Zunino G, et al. Early depolarizing GABA controls critical-period plasticity in the rat visual cortex. Nat Neurosci. 2014; 18:87-96. doi:10.1038/nn.3890

29. Wang DD, Kriegstein AR. Blocking early GABA depolarization with bumetanide results in permanent alterations in cortical circuits and sensorimotor gating deficits. Cereb Cortex. 2011; 21:574-587. doi:10.1093/cercor/bhq124

30. Dzhala V, Valeeva G, Glykys J, Khazipov R, Staley K. Traumatic alterations in GABA signaling disrupt hippocampal network activity in the developing brain. J Neurosci. 2012;32: 4017–4031. doi:10.1523/JNEUROSCI.5139-11.2012

31. Jaenisch N, Witte OW, Frahm C. Downregulation of potassium chloride cotransporter KCC2 after transient focal cerebral ischemia. Stroke. 2010;41: 151–159. doi:10.1161/STROKEAHA.109.570424

32. Edwards DH. Mechanisms of depolarizing inhibition at the crayfish giant motor synapse. I. Electrophysiology. J Neurophysiol. 1990;64:532-540. doi:10.1152/jn.1990.64.2.532

33. Staley KJ, Mody I. Shunting of excitatory input to dentate gyrus granule cells by a depolarizing GABA(A) receptor-mediated postsynaptic conductance. J Neurophysiol. 1992;68:197-212. doi:10.1152/jn.1992.68.1.197

34. Egawa K, Fukuda A. Pathophysiological power of improper tonic GABAAconductances in mature and immature models. Front Neural Circuits. 2013;7: 1–15. doi:10.3389/fncir.2013.00170

35. Ben-Ari Y, Gaiarsa JL, Tyzio R, Khazipov R. GABA: A pioneer transmitter that excites immature neurons and generates primitive oscillations. Physiol Rev. 2007;87: 1215–1284. doi:10.1152/physrev.00017.2006

36. Owens DF, Kriegstein AR. Is there more to GABA than synaptic inhibition? Nat Rev Neurosci. 2002;3: 715–727. doi:10.1038/nrn919

37. Jadi M, Polsky A, Schiller J, Mel BW. Location-dependent effects of inhibition on local spiking in pyramidal neuron dendrites. PLoS Comput Biol. 2012;8: e1002550. doi:10.1371/journal.pcbi.1002550

38. Spruston N, Stuart G, Häusser M. Principles of dendritic integration. in Dendrites (Spruston N, Stuart G, Häusser M eds.) 3rd edition, Oxford University Press, 2016. doi:10.1093/acprof:oso/9780198745273.003.0012

39. Gao XB, Chen G, Van Den Pol AN. GABA-dependent firing of glutamate-evoked action potentials at AMPA/kainate receptors in developing hypothalamic neurons. J Neurophysiol. 1998;79: 716–726. doi:10.1152/jn.1998.79.2.716

40. Gulledge AT, Stuart GJ. Excitatory actions of GABA in the cortex. Neuron. 2003;37: 299–309.

41. Howard MA, Rubel EW. Dynamic spike thresholds during synaptic integration preserve and enhance temporal response properties in the avian cochlear nucleus. J Neurosci. 2010;30-12063-12074. doi:10.1523/JNEUROSCI.1840-10.2010

42. Platkiewicz J, Brette R. A threshold equation for action potential initiation. PLoS Comput Biol. 2010;6: 25. doi:10.1371/journal.pcbi.1000850

43. Kolbaev SN, Achilles K, Luhmann HJ, Kilb W. Effect of depolarizing GABA A-mediated membrane responses on excitability of cajal-retzius cells in the immature rat neocortex. J Neurophysiol. 2011;106: 2034–2044. doi:10.1152/jn.00699.2010

44. Valeeva G, Abdullin A, Tyzio R, Skorinkin A, Nikolski E, Ben-Ari Y, et al. Temporal coding at the immature depolarizing gabaergic synapse. Front Cell Neurosci. 2010;4: 1–12. doi:10.3389/fncel.2010.00017

45. Kolbaev SN, Sharopov S, Dierkes PW, Luhmann HJ, Kilb W. Phasic GABAA-receptor activation is required to suppress epileptiform activity in the CA3 region of the immature rat hippocampus. Epilepsia. 2012;53: 888–896.

46. Murata Y, Colonnese MT. GABAergic interneurons excite neonatal hippocampus in vivo. Sci Adv. 2020;6: eaba1430. doi:10.1126/sciadv.aba1430

47. Flossmann T, Kaas T, Rahmati V, Kiebel SJ, Witte OW, Holthoff K, et al. Somatostatin Interneurons Promote Neuronal Synchrony in the Neonatal Hippocampus. Cell Rep. 2019;26: 3173-3182. doi: 10.1016/j.celrep.2019.02.061.

48. Kirmse K, Kummer M, Kovalchuk Y, Witte OW, Garaschuk O, Holthoff K. GABA depolarizes immature neurons and inhibits network activity in the neonatal neocortex in vivo. Nat Commun. 2015;6: 7750.

49. Lombardi A, Jedlicka P, Luhmann HJ, Kilb W. Giant depolarizing potentials trigger transient changes in the intracellular Cl - concentration in CA3 pyramidal neurons of the immature mouse hippocampus. Front Cell Neurosci. 2018;12:420. doi:10.3389/fncel.2018.00420

50. Kole MHP, Stuart GJ. Is action potential threshold lowest in the axon? Nat Neurosci. 2008;11: 1253–1255. doi:10.1038/nn.2203

51. Henze DA, Buzsáki G. Action potential threshold of hippocampal pyramidal cells in vivo is increased by recent spiking activity. Neuroscience. 2001;105: 121–130. doi:10.1016/S0306-4522(01)00167-1

52. Kolbaev SN, Mohapatra N, Chen R, Lombardi A, Staiger JF, Luhmann HJ, et al. NKCC-1 mediated Cl− uptake in immature CA3 pyramidal neurons is sufficient to compensate phasic GABAergic inputs. Sci Rep. 2020;10: 18399. doi:10.1038/s41598-020-75382-1

53. Ehrlich DE, Ryan SJ, Hazra R, Guo JD, Rainnie DG. Postnatal maturation of GABAergic transmission in the rat basolateral amygdale. J Neurophysiol. 2013;110: 926–941. doi:10.1152/jn.01105.2012

54. Leinekugel X, Khazipov R, Cannon R, Hirase H, Ben-Ari Y, Buzsáki G. Correlated Bursts of Activity in the Neonatal Hippocampus in Vivo. Science 2002;296: 2049–2052. doi:10.1126/science.1071111

55. Haider B, Duque A, Hasenstaub AR, McCormick DA. Neocortical network activity in vivo is generated through a dynamic balance of excitation and inhibition. J Neurosci. 2006;26: 4535–4545. doi:10.1523/JNEUROSCI.5297-05.2006

56. Pernía-Andrade AJ, Jonas P. Theta-Gamma-Modulated Synaptic Currents in Hippocampal Granule Cells InVivo Define a Mechanism for Network Oscillations. Neuron. 2014;81: 140–152. doi:10.1016/j.neuron.2013.09.046

57. Sipilä ST, Kaila K. GABAergic control of CA3-driven network events in the developing hippocampus. Results Probl Cell Differ. 2007;44: 99–121. doi:10.1007/400_2007_033

58. Rall W. Cable theory for dendritic neurons. In Koch C, Segev I (eds) Methods in Neuronal Modeling. MIT press 1989.

59. Stell BM, Mody I. Receptors with different affinities mediate phasic and tonic GABA(A) conductances in hippocampal neurons. J Neurosci. 2002;22:RC223. doi:20026399

60. Brickley SG, Mody I. Extrasynaptic GABA A Receptors: Their Function in the CNS and Implications for Disease. Neuron. 2012;73: 23–34. doi:10.1016/j.neuron.2011.12.012

61. Wright R, Raimondo J V, Akerman CJ. Spatial and Temporal Dynamics in the Ionic Driving Force for GABA(A) Receptors. Neural Plast. 2011; 2011:728395. doi: 10.1155/2011/728395

62. Bormann J, Hamill OP, Sakmann B. Mechanism of anion permeation through channels gated by glycine and gamma-aminobutyric acid in mouse cultured spinal neurones. J Physiol. 1987;385: 243–286. doi:10.1113/jphysiol.1987.sp016493

63. Fatima-Shad K, Barry PH. Anion permeation in GABA- and glycine-gated channels of mammalian cultured hippocampal neurons. Proc R Soc B Biol Sci. 1993;253: 69–75. doi:10.1098/rspb.1993.0083

64. Glykys J, Dzhala V, Egawa K, Balena T, Saponjian Y, Kuchibhotla K V, et al. Local Impermeant Anions Establish the Neuronal Chloride Concentration. Science. 2014;343: 670–675. Available: http://www.sciencemag.org/content/343/6171/670.abstract

65. Düsterwald KM, Currin CB, Burman RJ, Akerman CJ, Kay AR, Raimondo J V. Biophysical models reveal the relative importance of transporter proteins and impermeant anions in chloride homeostasis. Elife. 2018;7: 39575. doi:10.7554/eLife.39575

66. Jarolimek W, Lewen A, Misgeld U. A furosemide-sensitive K+-Cl- cotransporter counteracts intracellular Cl- accumulation and depletion in cultured rat midbrain neurons. J Neurosci. 1999;19: 4695–4704.

67. Raimondo JV, Markram H, Akerman CJ. Short-term ionic plasticity at GABAergic synapses. Front Synaptic Neurosci. 2012;4: 5. doi:10.3389/fnsyn.2012.00005

68. Currin CB, Trevelyan AJ, Akerman CJ, Raimondo J V. Chloride dynamics alter the input-output properties of neurons. PLoS Comput Biol. 2020;16: e1007932. doi:10.1371/journal.pcbi.1007932

69. Lombardi A, Jedlicka P, Luhmann HJ, Kilb W. Coincident glutamatergic depolarizations enhance GABAA receptor-dependent Cl- influx in mature and suppress Cl- efflux in immature neurons. PLOS Comput Biol. 2021;17: e1008573. doi:10.1371/journal.pcbi.1008573

70. Halbhuber L, Achtner C, Luhmann HJ, Sinning A, Kilb W. Coincident Activation of Glutamate Receptors Enhances GABAA Receptor-Induced Ionic Plasticity of the Intracellular Cl−-Concentration in Dissociated Neuronal Cultures. Front Cell Neurosci. 2019;13: 497. doi:10.3389/fncel.2019.00497

71. Luhmann HJ, Reiprich RA, Hanganu I, Kilb W. Cellular physiology of the neonatal rat cerebral cortex: Intrinsic membrane properties, sodium and calcium currents. J Neurosci Res. 2000;62: 574-584. doi:10.1002/1097-4547(20001115)62:4<574::AID-JNR12>3.0.CO;2-0

72. Doischer D, Hosp JA, Yanagawa Y, Obata K, Jonas P, Vida I, et al. Postnatal differentiation of basket cells from slow to fast signaling devices. J Neurosci. 2008;28: 12956–12968. doi:10.1523/JNEUROSCI.2890-08.2008

73. Isaacson JS, Scanziani M. How inhibition shapes cortical activity. Neuron. 2011;72: 231–243. doi:10.1016/j.neuron.2011.09.027

74. Jedlicka P, Deller T, Gutkin BS, Backus KH. Activity-dependent intracellular chloride accumulation and diffusion controls GABAA receptor-mediated synaptic transmission. Hippocampus. 2011;21: 885–898. doi:10.1002/hipo.20804

75. Kuner T, Augustine GJ. A genetically encoded ratiometric indicator for chloride: Capturing chloride transients in cultured hippocampal neurons. Neuron. 2000;27: 447–459. doi:10.1016/S0896-6273(00)00056-8

76. Staley KJ, Soldo BL, Proctor WR. Ionic mechanisms of neuronal excitation by inhibitory GABAA receptors. Science. 1995;269: 977–981. doi:10.1126/science.7638623

77. Freund TF. Interneuron Diversity series: Rhythm and mood in perisomatic inhibition. Trends Neurosci. 2003;26: 489–495. doi:10.1016/S0166-2236(03)00227-3

78. Elgueta C, Bartos M. Dendritic inhibition differentially regulates excitability of dentate gyrus parvalbumin-expressing interneurons and granule cells. Nat Commun. 2019;10: 5561. doi:10.1038/s41467-019-13533-3

79. Somogyi P, Klausberger T. Defined types of cortical interneurone structure space and spike timing in the hippocampus. J Physiol. 2005;562: 9–26. doi:10.1113/jphysiol.2004.078915

80. Ascoli GA, Alonso-Nanclares L, Anderson SA, Barrionuevo G, Benavides-Piccione R, Burkhalter A, et al. Petilla terminology: Nomenclature of features of GABAergic interneurons of the cerebral cortex. Nat Rev Neurosci. 2008;9: 557–568. doi:10.1038/nrn2402

81. Song I, Savtchenko L, Semyanov A. Tonic excitation or inhibition is set by GABAA conductance in hippocampal interneurons. Nat Commun. 2011;2: 310–376. doi:10.1038/ncomms1377

82. Andreozzi E, Carannante I, D'Addio G, Cesarelli M, Balbi P. Phenomenological models of NaV1.5. A side by side, procedural, hands-on comparison between Hodgkin-Huxley and kinetic formalisms. Sci Rep. 2019;9: 17493. doi:10.1038/s41598-019-53662-9

83. Milescu LS, Yamanishi T, Ptak K, Smith JC. Kinetic properties and functional dynamics of sodium channels during repetitive spiking in a slow pacemaker neuron. J Neurosci. 2010;30: 12113–12127. doi:10.1523/JNEUROSCI.0445-10.2010

84. Chizhov A V., Smirnova EY, Kim KK, Zaitsev A V. A simple Markov model of sodium channels with a dynamic threshold. J Comput Neurosci. 2014;37: 181–191. doi:10.1007/s10827-014-0496-6

Suppl. Data

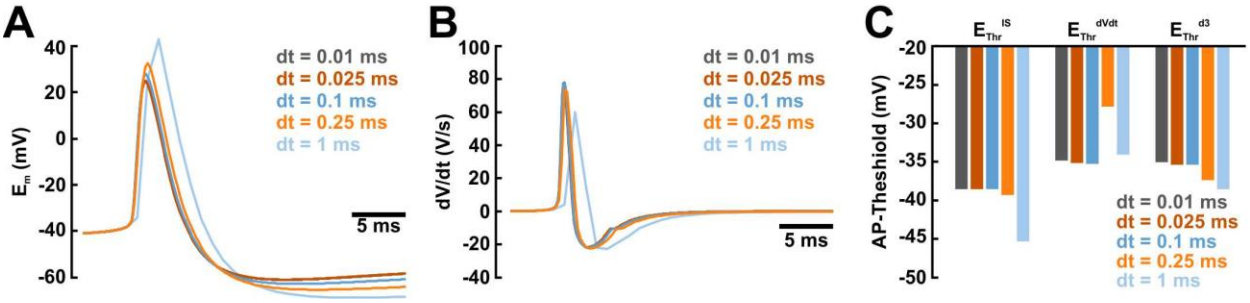

Suppl. Fig. 1. *Characterization of AP properties using different dt values for the simulation. A: Simulated voltage traces using different dt as indicated in the plot. Note the divergence of AP shape at larger dt values. B: Rate of E_m changes during an action potential. C: Typical $E_{AP}{}^{Thr}$ values determined with 3 different algorithms on the traces obtained at different dt. Note that all $E_{Thr}{}^{IS}$, $E_{Thr}{}^{dV/dt}$ and $E_{Thr}{}^{d3}$ remained stable for a dt ≤ 0.1 ms.*

Table 1

Phasic GABA - distributed GABA inputs					
g_{GABA}	p_{Max}	E_0	s	k	E_{GABA}^{Thr}
0.0158 pS	1 pS	-36.0 mV	-20.4 mV	0.75	-43.05 mV
0.0789 pS	1 pS	-37.7 mV	-2.5 mV	0.28	-43.35 mV
0.3945 pS	1 pS	-41.6 mV	-0.47 mV	0.21	-43.06 mV
Phasic GABA - proximal GABA inputs					
g_{GABA}	p_{Max}	E_0	s	k	E_{GABA}^{Thr}
0.0158 pS	1 pS	-38.5 mV	-19.3 mV	0.80	-43.32 mV
0.0789 pS	1 pS	-38.2 mV	-2.5 mV	0.30	-43.41 mV
0.3945 pS	1 pS	-41.8 mV	-0.49 mV	0.24	-43.12 mV
Phasic GABA - distal GABA inputs					
g_{GABA}	p_{Max}	E_0	s	k	E_{GABA}^{Thr}
0.0158 pS	1 pS	-39.5 mV	-22.3 mV	0.85	-43.10 mV
0.0789 pS	1 pS	-37.5 mV	-2.8 mV	0.30	-43.34 mV
0.3945 pS	1 pS	-41.45 mV	-0.6 mV	0.24	-43.09 mV
Tonic GABA					
g_{GABA}	p_{Max}	E_0	s	k	E_{GABA}^{Thr}
0.0875 pS	1.0 pS	-52.70 mV	-350.00 mV	1	-35.90 mV
0.1750 pS	1.0 pS	-49.60 mV	-226.00 mV	1	-38.75 mV
0.2625 pS	1.0 pS	-47.60 mV	-148.00 mV	1	-40.50 mV
0.4375 pS	1.0 pS	-46.10 mV	-87.00 mV	1	-41.93 mV
0.8750 pS	1.0 pS	-44.90 mV	-39.50 mV	1	-43.00 mV
1.7500 pS	1.0 pS	-24.30 mV	-17.50 mV	0.5	-43.41 mV
2.6250 pS	1.0 pS	-32.55 mV	-10.50 mV	0.5	-43.42 mV
4.3750 pS	1.0 pS	-36.95 mV	-6.20 mV	0.45	-43.59 mV
8.7500 pS	1.0 pS	-39.57 mV	-2.55 mV	0.38	-43.58 mV
17.5000 pS	1.0 pS	-41.34 mV	-1.17 mV	0.33	-43.55 mV
26.2500 pS	1.0 pS	-41.78 mV	-0.74 mV	0.29	-43.41 mV
43.7500 pS	1.0 pS	-42.26 mV	-0.48 mV	0.32	-43.20 mV
87.5000 pS	1.0 pS	-42.35 mV	-0.22 mV	0.3	-42.82 mV

Parameters used for the sigmoidal fit of the E_{GABA} to g_{GABA}^{Thr} relationship and the resulting $E_{GABA}Thr$.

990 **Table 2**

Parameter	Value	Description
Na^+ Channels		
$G^{Na}_{c\rightarrow o}$	0.65	Gain for Bolzmann-Function describing the $Na_c \rightarrow Na_o$ transition
$V^{Na}_{c\rightarrow o}$	-34.9	$V_{1/2}$ for Bolzmann-Function describing the $Na_c \rightarrow Na_o$ transition
$V^{Na}_{c\rightarrow o}$	-0.72	Slope for Bolzmann-Function describing the $Na_c \rightarrow Na_o$ transition
$G^{Na}_{o\rightarrow i}$	0.5	Gain for Bolzmann-Function describing the $Na_o \rightarrow Na_i$ transition
$V^{Na}_{o\rightarrow i}$	-34.9	$V_{1/2}$ for Bolzmann-Function describing the $Na_o \rightarrow Na_i$ transition
$V^{Na}_{o\rightarrow i}$	-0.9	Slope for Bolzmann-Function describing the $Na_o \rightarrow Na_i$ transition
$\Delta t^{Na}_{o\rightarrow i}$	0.51 ms	Time delay for the transition to become operational
$c^{dec}_{o\rightarrow i}$	0.1	Fraction of constantly decaying Na_o states
$G^{Na}_{i\rightarrow c}$	0.025	Gain for Bolzmann-Function describing the $Na_i \rightarrow Na_c$ transition
$V^{Na}_{i\rightarrow c}$	-20	$V_{1/2}$ for Bolzmann-Function describing the $Na_i \rightarrow Na_c$ transition
$V^{Na}_{i\rightarrow c}$	2.2	Slope for Bolzmann-Function describing the $Na_i \rightarrow Na_c$ transition
$G^{Na}_{c\rightarrow i}$	0.0001	Gain for Bolzmann-Function describing the $Na_c \rightarrow Na_i$ transition
$V^{Na}_{c\rightarrow i}$	-40	$V_{1/2}$ for Bolzmann-Function describing the $Na_c \rightarrow Na_i$ transition
$V^{Na}_{c\rightarrow i}$	-5	Slope for Bolzmann-Function describing the $Na_c \rightarrow Na_i$ transition
g_{Na}	0.0035 (S/cm^2)	Conductance density for Na^+ channels in the soma
E_{Na}	66 (mV)	Reversal potential for Na^+ currents
K^+ Channels		
$G^{K}_{c\rightarrow o}$	1.15	Gain for Bolzmann-Function describing the $K_c \rightarrow K_o$ transition
$V^{K}_{c\rightarrow o}$	-10	$V_{1/2}$ for Bolzmann-Function describing the $K_c \rightarrow K_o$ transition
$V^{K}_{c\rightarrow o}$	-2	Slope for Bolzmann-Function describing the $K_c \rightarrow K_o$ transition
Δt^{K}_{oci}	0.55 ms	Time delay for the transition to become operational
$G^{K}_{o\rightarrow c}$	0.055	Gain for Bolzmann-Function describing the $K_o \rightarrow K_i$ transition
$V^{K}_{o\rightarrow c}$	-10	$V_{1/2}$ for Bolzmann-Function describing the $K_o \rightarrow K_i$ transition
$V^{K}_{o\rightarrow c}$	1	Slope for Bolzmann-Function describing the $K_o \rightarrow K_i$ transition
Δt^{K}_{oci}	1.7 ms	Time delay for the transition to become operational
g_K	0.0006 (S/cm^2)	Conductance density for K^+ channels in the soma
E_K	-84 (mV)	Reversal potential for K^+ currents

991 *Parameters used for the modified Markov model.*